BIOCHEMISTRY

Defective import of mitochondrial metabolic enzyme elicits ectopic metabolic stress

Kazuya Nishio[1]†, Tomoyuki Kawarasaki[2]†, Yuki Sugiura[3,4]†, Shunsuke Matsumoto[5], Ayano Konoshima[2], Yuki Takano[2], Mayuko Hayashi[2], Fumihiko Okumura[6], Takumi Kamura[7]*, Tsunehiro Mizushima[1,8]*, Kunio Nakatsukasa[2]*

Deficiencies in mitochondrial protein import are associated with a number of diseases. However, although nonimported mitochondrial proteins are at great risk of aggregation, it remains largely unclear how their accumulation causes cell dysfunction. Here, we show that nonimported citrate synthase is targeted for proteasomal degradation by the ubiquitin ligase SCF^Ucc1. Unexpectedly, our structural and genetic analyses revealed that nonimported citrate synthase appears to form an enzymatically active conformation in the cytosol. Its excess accumulation caused ectopic citrate synthesis, which, in turn, led to an imbalance in carbon flux of sugar, a reduction of the pool of amino acids and nucleotides, and a growth defect. Under these conditions, translation repression is induced and acts as a protective mechanism that mitigates the growth defect. We propose that the consequence of mitochondrial import failure is not limited to proteotoxic insults, but that the accumulation of a nonimported metabolic enzyme elicits ectopic metabolic stress.

INTRODUCTION

Most mitochondrial proteins are synthesized as precursors with an N-terminal mitochondrial targeting sequence, also known as a presequence. During posttranslational import, these precursors are kept in an unfolded, import-competent state by cytosolic molecular chaperones to facilitate their passage through the translocator of the outer membrane (TOM) and translocator of the inner membrane (TIM) channels (1–4). However, the import process is affected by mitochondrial defects, problems in the cytosol, and cytosolic aggregation of pathological protein species including mutant huntingtin/ polyQ protein, α-synuclein, or β-amyloid (5–15).

The impairment of mitochondrial import results in an accumulation of nonimported proteins in the cytosol, an environment where there is a potential risk of misfolding due to the absence of suitable maturation factors. The accumulation of nonimported proteins in the cytosol may be toxic to the cell (16–19). To cope with these deleterious situations, cells have evolved various quality control mechanisms (6, 20–28), by which nonimported mitochondrial proteins are eliminated by the ubiquitin-proteasome system. Cells also respond to the accumulation of precursor proteins by suppressing mitochondrial precursor overaccumulation stress and by up-regulating proteasome and chaperone capacities (5, 18, 19).

When mitochondrial import is decreased, the mitochondrial protein uptake may be modulated by the import and translation machineries via the activation of the integrated stress response (ISR) (29).

The mechanism by which the accumulation of nonimported mitochondrial protein causes cellular dysfunction is poorly understood. It has been suggested that they may form toxic aggregates and/or associate with other proteins or organelles in the cell, thereby leading to proteostasis disturbance, cellular growth defects, or neurodegenerative diseases (15, 18, 19, 28, 30, 31). At the same time, sequestration of cytosolic molecular chaperones by nonimported precursor proteins may lead to a reduced protein-folding capacity and hence proteostatic stress, a situation that is related to aging and the development of various protein conformational diseases (5, 15).

In this study, to further elucidate how the accumulation of nonimported mitochondrial proteins exerts gain-of-function toxicity and cell dysfunction, we analyzed the consequence of the cytosolic accumulation of nonimported citrate synthase (Cit1), the first rate-limiting enzyme in the tricarboxylic/citrate acid (TCA) cycle. We demonstrate that cytosolic Cit1 is targeted for proteasomal degradation by the ubiquitin ligase complex SCF^Ucc1 (Skp1–Cdc53–F-box protein Ucc1). Our structural, biochemical, genetic, and metabolomics analyses demonstrate that, in contrast to the assumption that precursor proteins are kept in an unfolded, import-competent state in the cytosol, nonimported Cit1 almost certainly forms an enzymatically active conformation and that its accumulation exerts gain-of-function toxicity by synthesizing excess citrate in the cytosol. Intriguingly, under these conditions, translation repression is induced and acts as a protective mechanism against the ectopic citrate stress. These results suggest that the consequence of mitochondrial import failure is not limited to proteostatic insults, but that nonimported precursor proteins can elicit ectopic metabolic stress.

¹Department of Life Science, Graduate School of Science, University of Hyogo, 2167 Shosha, Himeji 671-2280, Japan. ²Graduate School of Science, Nagoya City University, Yamanohata 1, Mizuho-cho, Mizuho-ku, Nagoya, Aichi 467-8501, Japan. ³Department of Biochemistry, School of Medicine, Keio University, 35 Shinanomachi, Shinjuku-ku, Tokyo 160-8582, Japan. ⁴Multiomics Platform, Center for Cancer Immunotherapy and Immunobiology, Kyoto University Graduate School of Medicine, Kyoto 606-8501, Japan. ⁵Department of Bioscience and Biotechnology, Graduate School of Bioresource and Bioenvironmental Sciences, Kyushu University, Motooka 744, Nishi-ku, Fukuoka 819-0395, Japan. ⁶Department of Food and Health Sciences, International College of Arts and Sciences, Fukuoka Women's University, Fukuoka 813-8582, Japan. ⁷Division of Biological Sciences, Graduate School of Science, Nagoya University, Nagoya, Aichi 464-8602, Japan. ⁸Graduate School of Pharmaceutical Sciences, Nagoya City University, 3-1 Tanabe-dori, Mizuho-ku, Nagoya 467-8603, Japan.
†These authors contributed equally to this work.
*Corresponding author. Email: nakatsukasa@nsc.nagoya-cu.ac.jp (K.N.); mizushi@sci.u-hyogo.ac.jp (T.M.); kamura.takumi.k1@f.mail.nagoya-u.ac.jp (T.K.)

RESULTS

The F-box protein Ucc1 discriminates the relatively subtle but refined structural changes of citrate synthase

While citrate is mainly produced in the mitochondria, cytosolic citrate can be supplied from the mitochondria and from the extracellular environment and is also crucial for epigenetic regulation and fatty acid synthesis (32). In plants and fungi, cytosolic citrate is also supplied via the glyoxylate cycle, a cytosolic/peroxisomal gluconeogenic pathway that is similar to the TCA cycle (33). We demonstrated previously that Cit2, a cytosolic and peroxisomal citrate synthase in the glyoxylate cycle, is targeted for proteasomal degradation by the SCF^{Ucc1} ubiquitin ligase and that the SCF^{Ucc1}-mediated degradation of Cit2 acts as a metabolic switch for the glyoxylate cycle (34). The importance of Ucc1-mediated degradation of Cit2 in maintaining citrate homeostasis is underscored by the fact that Ucc1 exhibits negative genetic interactions with a number of mitochondrial enzymes including Idh1, the mitochondrial isocitrate dehydrogenase (www.yeastgenome.org/) (34). To investigate the mechanism by which Ucc1, a substrate recognition subunit, recognizes citrate synthase, we performed an x-ray crystal structure analysis. Instead of peptides that are commonly used to mimic the substrate proteins (35), we succeeded in determining the structure of Ucc1-Skp1 in a complex with full-length Cit2 at a 2.30-Å resolution (Fig. 1A). The electron densities of the N-terminal region of Skp1 (residues 1 to 84 and 97 to 112) were not visible in this complex (Fig. 1A). However, when a nonessential loop (residues 37 to 64), which was previously suggested to interfere with crystallization (36), was deleted from Skp1, we were able to obtain a more complete structure, with a resolution of 2.53 Å (fig. S1, A and B). The Cit2-Ucc1-Skp1 complex structure contained one Ucc1-Skp1 complex and one Cit2 dimer (Fig. 1A). This quaternary complex had a curved structure in which Skp1 and Cit2 were located at the opposite ends of Ucc1. In addition, Ucc1 held one of two Cit2 molecules [Cit2(A) in Fig. 1A]. Ucc1 contains a typical F-box domain at its N terminus, but other regions formed a unique structure with no known motifs (35, 37).

At the interaction surface, the H14 and H20 helices in Cit2 are associated with the H9 and H10 helices in Ucc1, respectively, and the H6-H7 loop in Cit2 is associated with the S10 strand in Ucc1 (Fig. 1B). The interaction surface of Ucc1 and Cit2 comprised complementary charged residues (fig. S1C). Among the residues located on these surfaces, D154 and E309 in Cit2 were predicted to form salt bridges with K345 and R184 in Ucc1, respectively, while E309 and S409/S410 in Cit2 were predicted to form hydrogen bonds with Y185 and E212 in Ucc1, respectively (Fig. 1B). Mutant Cit2 variants harboring a D154A, E309A, or S409A/S410A substitution displayed reduced binding to Ucc1 (Fig. 1C). Similarly, mutant Ucc1 variants harboring R184A/Y185A, E212A, or K345A substitutions displayed reduced binding to Cit2 (Fig. 1D). Consistent with these findings, Cit2 was stabilized almost completely in cells expressing Ucc1 mutants (R184A/Y185A or K345A) that were defective in Cit2 recognition (fig. S1D).

The structure of Cit2 in the Ucc1-Skp1-Cit2 quaternary complex was almost identical to that of the open form of Cit2 [Apo-Cit2(A)] shown in Fig. 1E. This form is free from its substrates oxaloacetate (OAA) and acetyl-CoA. We also determined the crystal structure of the closed form of Cit2 in complex with OAA and CoA. Here, CoA was used instead of acetyl-CoA to prevent the reaction during crystallization. We found that in the presence of OAA and CoA, Cit2 undergoes a ligand-induced conformational change that includes movement of E309, resulting in the destruction of both a hydrogen bond between E309 in Cit2 and Y185 in Ucc1 and the salt bridge between E309 in Cit2 and R184 in Ucc1 (fig. S2A). Perhaps more critically, this conformational change also involves a large movement of helix 14 in Cit2, resulting in steric hindrance that likely prevents recognition by Ucc1 (fig. S2, A to C). Ucc1 preferentially recognized the open (ligand-free) form but not the closed (ligand-bound) enzyme (fig. S2D). These results suggest that, in contrast to the canonical degron-mediated substrate recognition that occurs for other well-studied F-box proteins, such as Fbw7, Cdc4, β-TrCP1, and Skp2 (36, 38–40), Ucc1 discriminates the relatively subtle but refined structural changes that are induced upon of substrate binding during catalysis. This arises as a result of complementary polar interfaces through hydrogen bonds and salt bridges. Moreover, these results provide a structural basis for the previously proposed positive feedback loop in which a higher amount of gluconeogenic metabolites (e.g., acetyl-CoA and OAA) stabilizes Cit2 to further activate the glyoxylate cycle (34).

Nonimported mitochondrial citrate synthase is targeted for proteasomal degradation by the SCF^{Ucc1} ubiquitin ligase complex

Cit2 shares 75.6% primary sequence identity and 86.7% similarity with Cit1, a mitochondrial citrate synthase (fig. S3A). We solved the crystal structure of Apo-Cit1, and it was almost identical to that of Apo-Cit2 (Fig. 2A). We therefore reasoned that nonimported Cit1 in the cytosol could also be targeted for proteasomal degradation via SCF^{Ucc1}. To test this hypothesis, we first constructed a Cit1 mutant that lacked amino acids 2 to 42, the region containing the N-terminal mitochondrial targeting sequence (hereafter, we call this mutant NΔCit1) (Fig. 2, B and C). Green fluorescent protein (GFP)–tagged NΔCit1 was localized in the cytosol (Fig. 2D). The cytosolic localization of NΔCit1 was further confirmed by subcellular fractionation analysis (Fig. 2D). To assess the stability of NΔCit1, we performed a cycloheximide chase experiment and found that NΔCit1 was degraded with a half-life of ~45 min but was stabilized by the addition of the proteasome inhibitor MG132 (Fig. 2E and fig. S3B). We also found that NΔCit1 degradation was attenuated in temperature-sensitive *cdc34-2*, *cdc53-1*, and *skp1-11* mutant cells and in cells lacking Ucc1 (Fig. 2, F and G, and fig. S3, C, and D). Moreover, NΔCit1, but not the mitochondrial form of mature Cit1 (mtCit1), was ubiquitinated in a Ucc1-dependent manner in vivo (Fig. 2H). Together, these results demonstrate that NΔCit1 is ubiquitinated by SCF^{Ucc1} for proteasomal degradation.

Next, we analyzed the physical interaction between Ucc1 and NΔCit1 using a pull-down assay. An anti-FLAG affinity gel loaded with the recombinant 3xFLAG-Ucc1-Skp1 complex was incubated with yeast lysate prepared from cells expressing hemagglutinin (HA)–tagged Cit1 or NΔCit1. As shown in Fig. 2I, NΔCit1 is bound to the 3xFLAG-Ucc1-Skp1 complex (lane 3). Direct binding was confirmed by a pull-down assay with purified recombinant maltose binding protein (MBP)–tagged Cit1 and the Ucc1-Skp1 complex (Fig. 2J, lane 9). In addition, direct binding between purified MBP-Cit2 and the Ucc1-Skp1 complex was confirmed in the same experiment (lane 10). We noticed that when whole-cell lysate containing Cit1 was used in the lysate-based pull-down
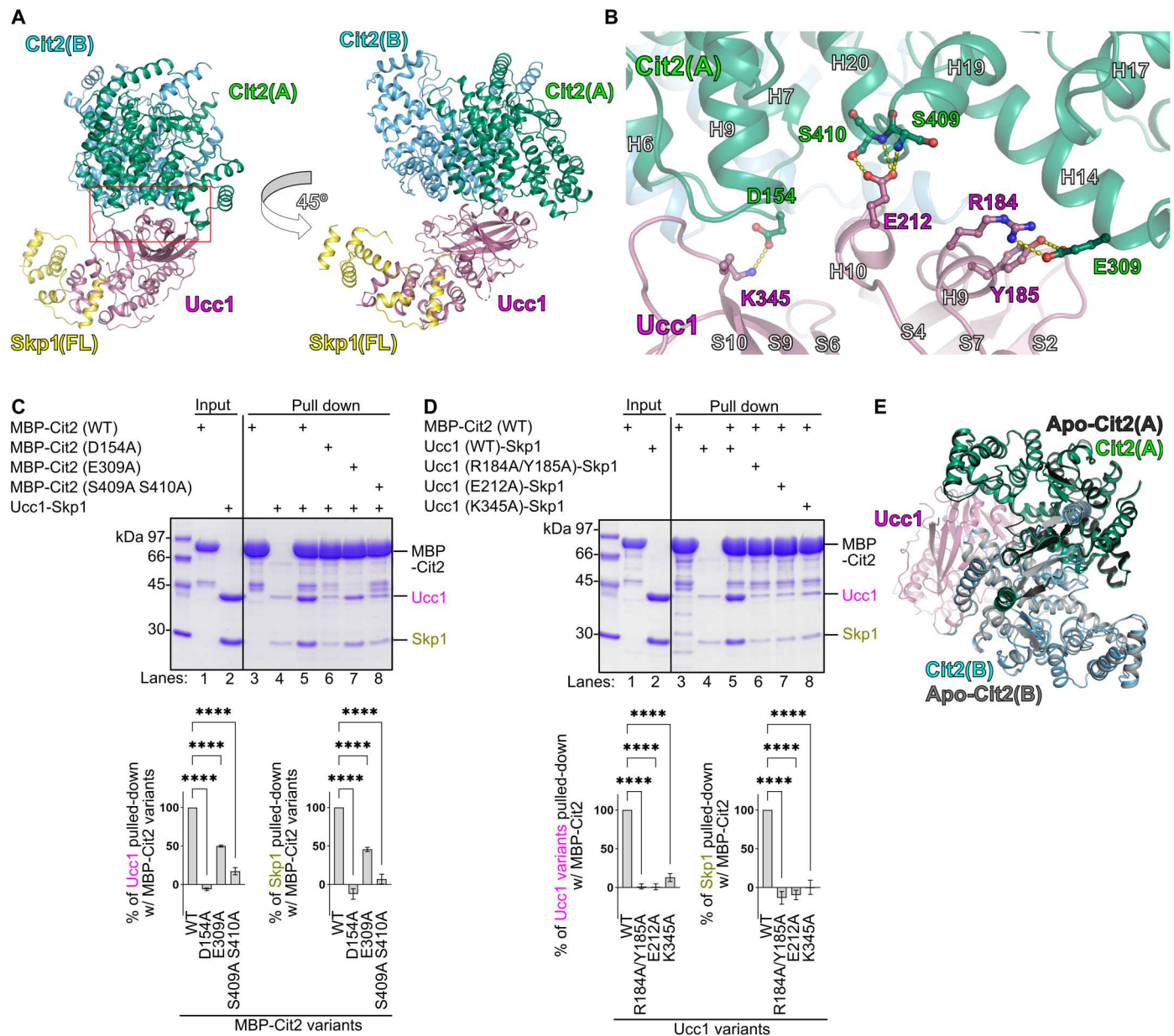
Fig. 1. Structural basis for the recognition of citrate synthase by the Ucc1-Skp1 complex. (**A**) Ribbon representation of the complex comprising the Cit2 dimer [Cit2(A), green; Cit2(B), cyan], Ucc1 (magenta), and full-length Skp1 [Skp1(FL), yellow] in two different side-view orientations. Ucc1 associates with Cit2(A). (**B**) Intermolecular contacts between Cit2 and Ucc1 in the Cit2-Ucc1-Skp1 complex. Enlarged view of the contacts shown in the red box in (A). Ribbon representation of the Cit2(A) monomer (green) and Ucc1 (magenta). Critical hydrogen bonding residues are shown as sticks, with hydrogen bonds as broken yellow lines. (**C**) Interaction between Ucc1-Skp1 and MBP-Cit2 or its mutant derivatives was analyzed using a pull-down assay with purified proteins. Amylose resin loaded with MBP-Cit2 or its mutant derivatives was incubated with an equal amount of the Ucc1-Skp1 complex purified from bacteria. Ucc1 and Skp1 bound to MBP-Cit2 were quantified. The amounts of Ucc1 and Skp1 bound to wild-type (WT) MBP-Cit2 (lane 5) were set to 100%. Data in the graph represent the means ± SE of five independent experiments; ****$P < 0.0001$, one-way analysis of variance (ANOVA) with Dunnett's multiple comparison test. (**D**) Same experiment as shown in (C), with the exception that Ucc1 and its mutant derivatives were used. The amounts of WT Ucc1 and Skp1 bound to MBP-Cit2 (lane 5) were set to 100%. Data in the graph represent the means ± SE of four independent experiments; ****$P < 0.0001$, one-way ANOVA with Dunnett's multiple comparison test. (**E**) Superposition of the dimers of Apo-Cit2 alone [Apo-Cit2(A), black; Apo-Cit2(B), gray] and Cit2 in complex with Ucc1 [Cit2(A), green; Cit2(B), cyan; Ucc1, magenta].
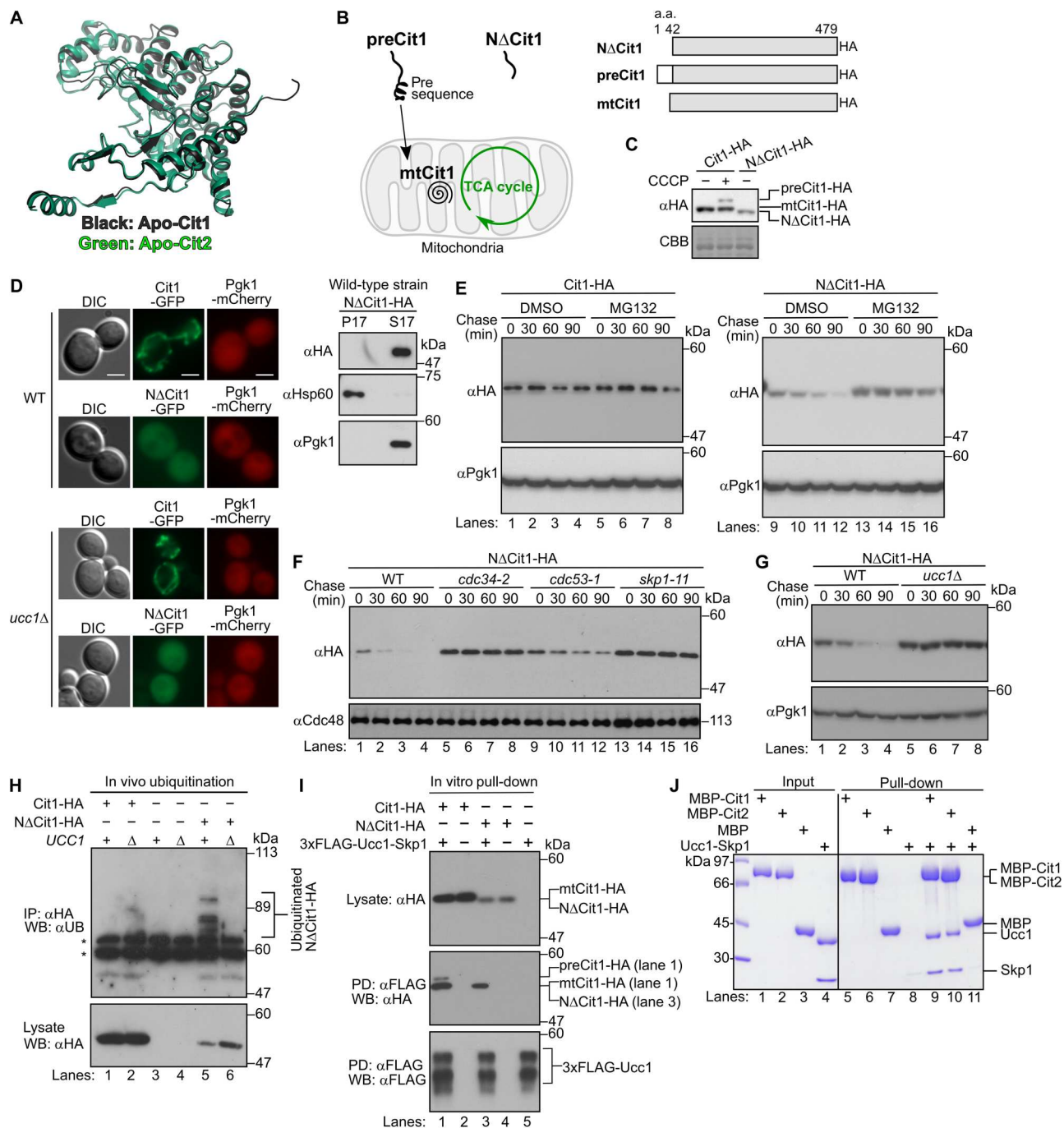
Fig. 2. NΔCit1 is degraded by the proteasome in an SCF^Ucc1 ubiquitin ligase-dependent manner. (**A**) Comparison of the structures of Apo-Cit1 (black) and Apo-Cit2 (green). (**B**) Schematic illustration of preCit1, NΔCit1, and mtCit1 constructs. (**C**) Cells expressing WT Cit1-HA or NΔCit1–hemagglutinin (HA) were treated with (+) or without (−) carbonyl cyanide *m*-chlorophenyl hydrazine (CCCP). Coomassie brilliant blue (CBB) staining of the membrane served as a loading control. (**D**) Subcellular localization of NΔCit1. Microscopic analysis of Cit1-GFP and NΔCit1-GFP in WT and *ucc1*Δ cells (left). Pgk1-mCherry served as a cytosolic marker. DIC, Differential Interference Contrast. Scale bars, 2 μm. Subcellular fractionation analysis of NΔCit1 (right). Hsp60 and Pgk1 served as mitochondrial and cytosolic markers, respectively. (**E**) Stabilities of mtCit1-HA and NΔCit1-HA were assessed by cycloheximide chase analysis in the presence or absence of the proteasome inhibitor MG132. Pgk1 served as a loading control. Quantified results for NΔCit1-HA (*n* = 3) are shown in fig. S3B. DMSO, dimethyl sulfoxide. (**F**) Stability of NΔCit1-HA was assessed by cycloheximide chase analysis in the indicated temperature-sensitive strains. Cdc48 served as a loading control. Quantified results (*n* = 3) are shown in fig. S3C. (**G**) Stability of NΔCit1-HA was analyzed in *ucc1*Δ cells. Pgk1 served as a loading control. Quantified results (*n* = 3) are shown in fig. S3D. (**H**) In vivo ubiquitination states of mtCit1-HA and NΔCit1-HA were analyzed in the indicated strains. Asterisks indicate immunoglobulin G (IgG) and/or nonspecific bands. IP, immunoprecipitation; WB, western blotting. (**I**) Interaction between 3xFLAG-Ucc1-Skp1 and Cit1-HA or NΔCit1-HA was analyzed using a lysate-based pull-down assay. PD, pull-down. Note that 3xFLAG-Ucc1-Skp1 appears as two bands (PD, αFLAG; WB, αFLAG), possibly due to processing in host insect cells (*34*). (**J**) Interaction between Ucc1-Skp1 and MBP-Cit1 or MBP-Cit2 was analyzed as in Fig. 1C. The bound proteins were analyzed by CBB staining of SDS–polyacrylamide gel electrophoresis (SDS-PAGE) gel.

assay, the mature mitochondrial form of Cit1 (mtCit1) was pulled down with the 3xFLAG-Ucc1-Skp1 complex (Fig. 2I, lane 1, faster migrating band in the middle panel). This finding is most likely explained by detergent-induced solubilization of mtCit1 from the mitochondrial matrix into the lysate fraction and its subsequent binding to Ucc1. Notably, the slower migrating band, which corresponded to the presequence-containing precursor form of Cit1 (preCit1), was also enriched by pull down with the 3xFLAG-Ucc1-Skp1 complex (lane 1 in the middle panel), although it was barely detectable in whole-cell lysate (lane 1 in the top panel). This result raised the intriguing possibility that preCit1 could also be recognized by the SCF[Ucc1] complex for degradation (see below).

Although the crystal structure of the Skp1-Ucc1-Cit1 complex is currently unknown, we found that the amino acid residues in Cit2 that were predicted to be critical for Ucc1 binding were conserved in Cit1 (Fig. 3A and fig. S3A). When D173 and S429 of NΔCit1, which correspond to D154 and S410 in Cit2, respectively, were simultaneously mutated to alanine, the resultant mutant (hereafter referred to as NΔCit1-DS/AA) was no longer recognized and ubiquitinated by Ucc1 (Fig. 3B, lane 3; Fig. 3C, lane 3). Consistent with these results, a cycloheximide chase experiment demonstrated that NΔCit1-DS/AA was stable in wild-type (WT) cells (Fig. 3D, lanes 17 to 20) to the same extent as NΔCit1 in $ucc1\Delta$ cells (lanes 5 to 8). These results demonstrate that presequence-lacking, nonimported Cit1 (NΔCit1) is recognized and ubiquitinated by the SCF[Ucc1] complex for proteasomal degradation. Moreover, our results also suggest that Ucc1 appears to recognize the folded citrate synthase because the amino acid residues critical for Ucc1 binding are assembled on the same surface in the three-dimensional structure although they are located distantly in the primary sequence (figs. S1C and S3A).

NΔCit1 toxicity depends on enzymatic activity

To examine the physiological significance of SCF[Ucc1]-mediated degradation of nonimported Cit1, we analyzed the growth of cells in which NΔCit1 accumulated in the cytosol. Cells overexpressing NΔCit1 under the control of the $GAL1$ promoter grew somewhat slower than control cells harboring empty plasmids (Fig. 4A, compare lines 1 and 3). The growth defect phenotype caused by NΔCit1 expression was exacerbated when $UCC1$ was deleted (Fig. 4A, line 6) or when DS/AA mutations were introduced into NΔCit1 (Fig. 4B, line 2), suggesting that toxicity is dose dependent. By contrast, cells overexpressing WT Cit1 grew robustly to the same extent as control cells, regardless of the presence or absence of Ucc1 or the DS/AA mutations (Fig. 4A, lines 2 and 5, and fig. S4A). The NΔCit1 growth phenotype was more pronounced in another genetic background (fig. S4, B and C), yet NΔCit1 toxicity was apparent even when expressed at endogenous levels (fig. S4B). Similar to the results obtained with NΔCit1, the overexpression of Cit2
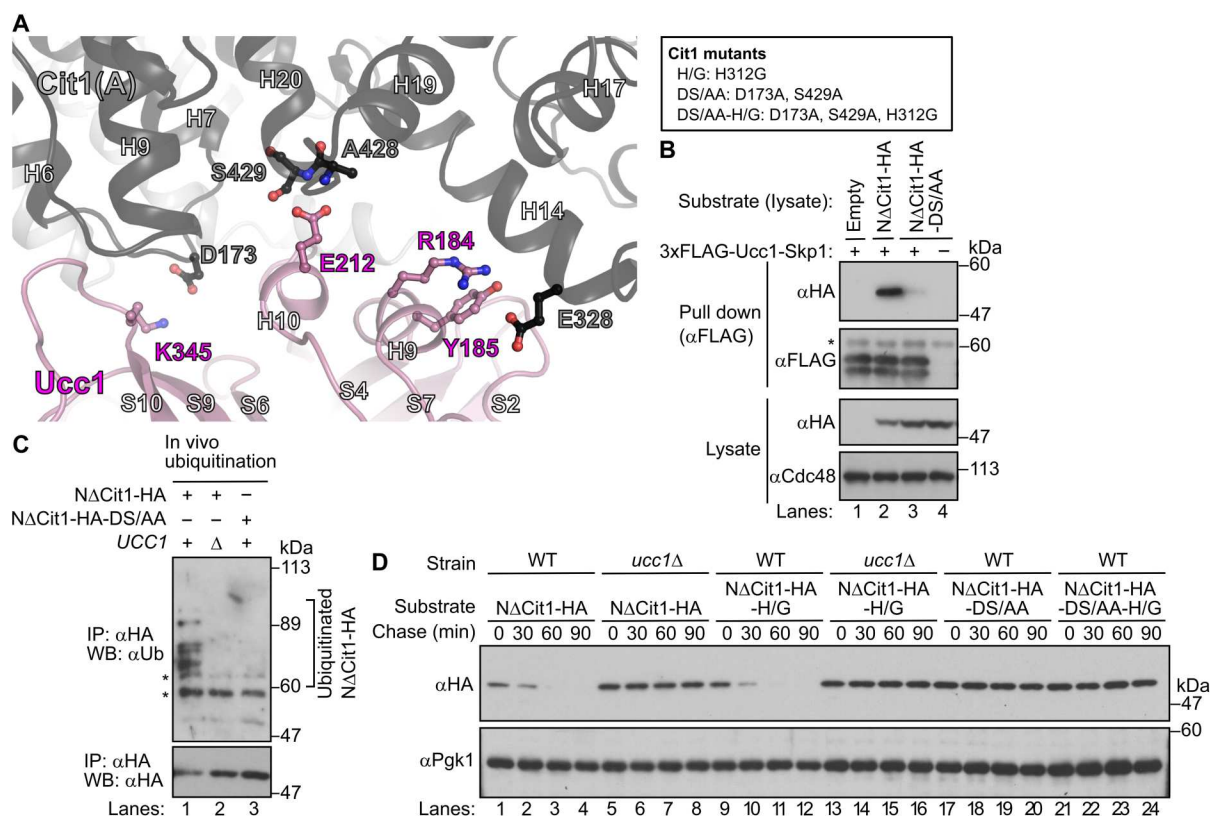

Fig. 3. Ucc1 recognizes folded citrate synthase via its conserved amino acids. (**A**) Predicted intermolecular contacts between Apo-Cit1 and Ucc1. Apo-Cit1 was superimposed on Cit2 in the Cit2-Ucc1-Skp1 complex. Apo-Cit1 and Ucc1 are depicted in black and magenta, respectively. Conserved amino acids predicted to form hydrogen bonds are shown as stick models. (**B**) Interactions between 3xFLAG-Ucc1-Skp1 and NΔCit1-HA or NΔCit1-HA-DS/AA were analyzed using a lysate-based pull-down assay, as described for Fig. 2I. Cdc48 served as loading controls for lysate preparation. Asterisk indicates IgG. (**C**) In vivo ubiquitination states of NΔCit1-HA in WT or $ucc1\Delta$ cells (lanes 1 and 2), and NΔCit1-HA-DS/AA in WT cells (lane 3) were analyzed in the indicated strains. Asterisks indicate IgG and/or nonspecific bands. (**D**) Stabilities of NΔCit1-HA and its mutant derivatives were assessed using a cycloheximide chase analysis. Pgk1 served as a loading control.
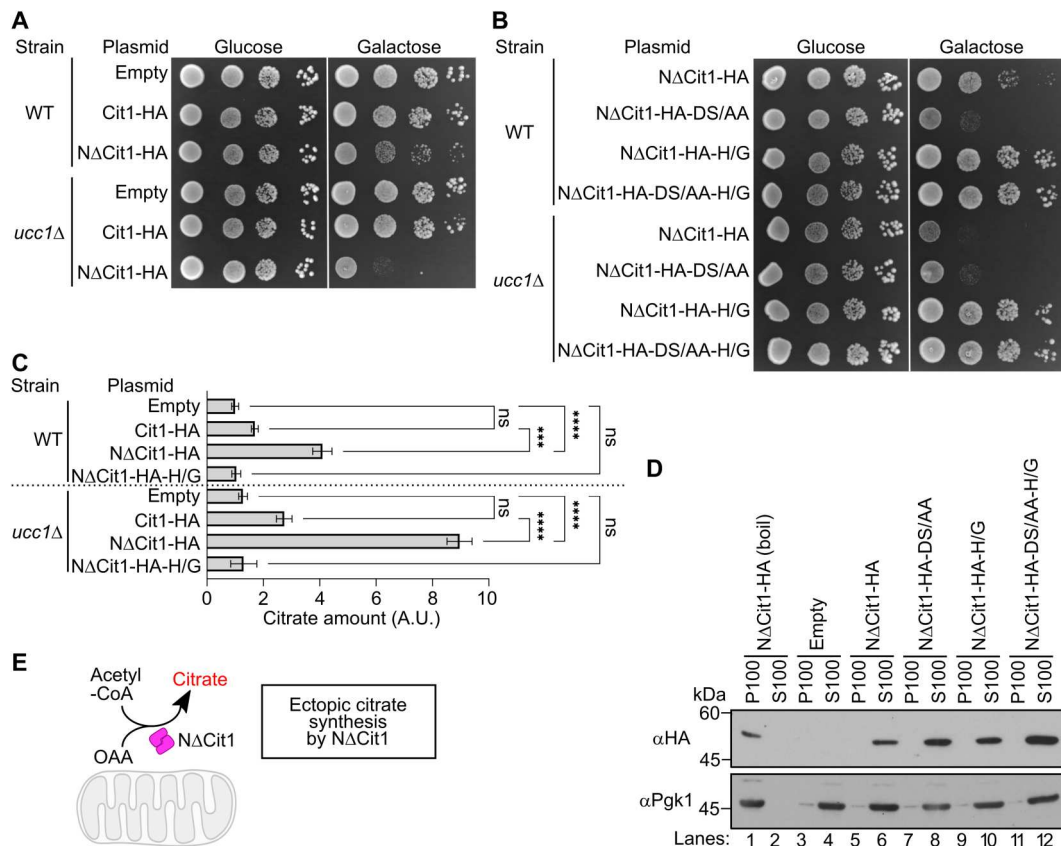
Fig. 4. Accumulation of NΔCit1 in the cytosol is toxic to cells in an enzymatic activity–dependent manner. (**A** and **B**) Ten-fold serial dilutions of the WT and *ucc1Δ* strains were spotted on SD (glucose) or SGal (galactose) medium. Cit1-HA, NΔCit1-HA, and mutant derivatives of NΔCit1-HA were expressed under the control of the *GAL1* promoter. Cells were grown at 30°C for 2 to 3 days. (**C**) Cellular citrate levels were measured in WT and *ucc1Δ* cells expressing Cit1-HA, NΔCit1-HA, or NΔCit1-HA-H/G. Values are arbitrary units (A.U.), and the amount of citrate in WT cells harboring empty vector was set to 1.0. Data represent the means ± SE of three independent experiments; ns, not significant; ***$P < 0.001$ and ****$P < 0.0001$, one-way ANOVA with Bonferroni's multiple comparison test. (**D**) Solubilities of NΔCit1-HA and its mutant variants expressed in WT cells were analyzed by ultracentrifugation at 100,000*g* for 1 hour at 4°C in the presence of 1% Triton X-100. Where indicated, the lysate was heated at 100°C (boil), and the supernatant (S100) and pellet (P100) fractions were subjected to SDS-PAGE analysis. Blots for Pgk1 (soluble protein) are shown. (**E**) Schematic representation of ectopic citrate synthesis caused by NΔCit1.

under the control of the *GAL1* promoter in *ucc1Δ* cells also impaired growth (fig. S4D), suggesting that there is not a substantial difference between NΔCit1 and Cit2 as enzymes in the cytosol.

Because our structural analysis demonstrated that Ucc1 recognizes only folded citrate synthase, we hypothesized that NΔCit1 forms an enzymatically active conformation in the cytosol. NΔCit1 rescued a glutamate auxotrophic phenotype of *cit1Δcit2Δ* cells (fig. S4E) (*34*, *41*), indicating that it maintains citrate synthase activity in the cytosol. The citrate synthase activity of NΔCit1 was also confirmed by directly measuring cellular citrate (Fig. 4C, line 3). In addition, *ucc1Δ* cells expressing NΔCit1 or WT cells expressing NΔCit1-DS/AA accumulated more citrate than WT cells or those expressing NΔCit1 (Fig. 4C, line 7, and fig. S4F). By contrast, when histidine 312 (fig. S3A), which is critical for citrate synthase activity (*42*, *43*), was mutated to glycine, the citrate synthase activities of NΔCit1 and NΔCit1-DS/AA were nearly eliminated (Fig. 4C, lines 4 and 8, and fig. S4F). In addition, the H/G mutation eliminated the growth defect phenotype caused by the accumulation of NΔCit1 or NΔCit1-DS/AA (Fig. 4B, lines 3, 4, 7, and 8), indicating that NΔCit1 toxicity arises from enzymatic activity. It should be noted that the H/G mutation did not affect the half-lives of the

NΔCit1 and NΔCit1-DS/AA variants (Fig. 3D, lanes 9 to 16 and 21 to 24), suggesting that lower citrate levels and the elimination of the growth defect phenotype were not due to a reduction in protein levels. We also noted that NΔCit1 and its variants were soluble and did not form insoluble aggregates in cells (Fig. 4D). Overall, these results demonstrate that the cellular toxicity of ectopically accumulated citrate synthase depends on its enzymatic activity (Fig. 4E).

Intriguingly, cells expressing Cit1, most of which is imported into the mitochondria and becomes the mature form (mtCit1), exhibited lower citrate levels than those expressing NΔCit1 (Fig. 4C; compare lines 2 to 3 and lines 6 to 7). This is most likely because citrate produced by mtCit1 in the mitochondria might be rapidly consumed by enzymes in the TCA cycle, while citrate produced by NΔCit1 might be consumed to a lesser degree. We note that adenosine triphosphate citrate lyase, which breaks citrate down to acetyl-CoA and OAA, has not been found in *Saccharomyces cerevisiae* (*44*). It is also possible that the availability of mitochondrial component(s) that regulate mtCit1 activity (*45*) might be limited in the cytosol.

preCit1 toxicity depends on enzymatic activity

Thus far, our studies were based on a mutant that lacked the mitochondrial targeting sequence (Fig. 5A, left), an element that would be retained in bona fide mislocalized proteins caused by mitochondrial import failure. To investigate the stability of presequence-containing Cit1, we used a *tom40-97* temperature-sensitive mutant (Fig. 5A, right) (*46*). The *tom40-97* allele carries a single-point mutation (W243R) that results in ineffective transfer of precursors to the TIM23 complex (*46*). When Cit1 was overexpressed in *tom40-97* cells, preCit1 accumulated (Fig. 5B, lane 1) and was degraded over time (lanes 1 to 4). Although we were unable to create *tom40-97ucc1Δ* cells due to the unknown difficulty of genetic manipulation for this strain, we found that preCit1-DS/AA was stable (Fig. 5B, lanes 5 to 12), suggesting that preCit1 degradation depends on Ucc1. A similar trend was observed when Cit1 was expressed under the control of its own promoter (fig. S5A). We note that the precursor form of Hsp60 that accumulated in *tom40-97* cells remained constant during the chase period (Fig. 5B). This observation emphasizes the specificity of precursor protein quality control. The Ucc1-dependent degradation of preCit1 was also observed in cells when import was blocked by a "clogger," b2(220)–dihydrofolate reductase (DHFR), which is imported into mitochondria slowly and thus competes with the import of other precursor proteins (fig. S5, B to F) (*5*).

Next, we investigated whether the accumulation of preCit1 using this alternate system is also toxic, with toxicity depending on enzymatic activity (see above). When Cit1 was overexpressed under the control of the *GAL1* promoter, *tom40-97* cells grew almost as well as control cells harboring an empty plasmid at both a permissive temperature of 26°C and a restrictive temperature of 35°C (Fig. 5C, lines 6 and 7). However, *tom40-97* cells expressing Cit1-DS/AA, which escapes Ucc1-mediated degradation, grew more slowly than cells harboring an empty plasmid at 35°C (Fig. 5C, lines 6 and 8). A similar trend was observed when cells were grown in liquid medium at a semipermissive temperature of 30°C (Fig. 5, D and E). The growth defect phenotype of *tom40-97* yeast expressing Cit1-DS/AA was canceled by introduction of the H/G mutation that eliminates activity (Fig. 5C, line 10; Fig. 5E). Consistent with these results, a greater level of citrate was present in *tom40-97* cells expressing Cit1-DS/AA than in those expressing Cit1 or Cit1-DS/AA-H/G (Fig. 5F and fig. S5G). Similarly, in cells expressing b2(220)-DHFR, the deletion of *UCC1* resulted in higher accumulation of citrate (fig. S5H). In this experiment, *CIT2* was deleted to exclude the effect caused by its accumulation upon loss of Ucc1. This data suggests that preCit1 expressed from the purely endogenous locus can exhibit enzymatic activity when it accumulates in the cytosol upon import failure.

Because Ucc1 recognizes folded citrate synthase (Figs. 1 and 3), the fact that nonimported preCit1 is recognized and targeted for degradation by Ucc1 (Figs. 2I and 5B, and fig. S5) suggests that preCit1 likely folds into a three-dimensional conformation similar to NΔCit1, which is catalytically active in the cytosol, although further analysis is required to fully prove whether preCit1 forms a dimer in the cytosol in vivo. This notion was supported by the observation that preCit1-DS/AA was soluble (Fig. 5G). Moreover, accumulation of enzymatically active citrate synthase was more toxic in the cytosol than in the mitochondria (Fig. 4 and fig. S4). On the basis of these results, we propose that the growth defect of *tom40-97*

cells expressing Cit1-DS/AA (Fig. 5, C to E) can be ascribed to cytosolic citrate synthesis by nonimported preCit1.

The idea that preCit1 in the cytosol can affect cellular activity was also supported by competitive growth analysis (*47*). In this experiment, we used *pam17Δ* cells, which are defective in import of select matrix-targeted precursors (*48*). Cells overexpressing WT Cit1 under the control of the *GAL1* promoter displayed better fitness than those expressing Cit1-DS/AA, suggesting that Ucc1-mediated degradation of preCit1 is crucial for cellular homeostasis (fig. S5, I and J). Cells expressing WT Cit1 under the control of the *CIT1* (native, physiological) promoter displayed slightly better fitness than those expressing Cit1-DS/AA (fig. S5, K and L), although the difference was not statistically significant. By contrast, when these cells were grown in synthetic "minimum" medium containing only necessary amino acids, cells expressing WT Cit1 displayed lower fitness than those expressing Cit1-DS/AA (fig. S5M), suggesting that moderate accumulation of preCit1 can increase or decrease cellular fitness depending on the environment. Regardless, these results further support our idea that preCit1 that accumulates in the cytosol exhibits enzymatic activity upon import failure and affects cellular activity.

Ectopic citrate synthesis triggers metabolic imbalance

Our data suggest that ectopic citrate synthesis by nonimported Cit1 represents a form of metabolic perturbation, one that might mimic the consequence of mitochondrial import failure, for example, in cancer cells that overexpress citrate synthase (*49–51*). To comprehensively evaluate the impact of cytosolic citrate synthesis on metabolism, we compared the metabolomic profiles of WT cells expressing NΔCit1-DS/AA and NΔCit1-DS/AA-H/G (Fig. 6A, left, comparison I) and those of *tom40-97* cells expressing Cit1-DS/AA and Cit1-DS/AA-H/G (Fig. 6A, right, comparison II). For this purpose, cationic and anionic metabolites were comprehensively quantified by liquid chromatography–mass spectrometry (LC-MS) and ion chromatography–MS (IC-MS), respectively. We showed that citrate was accumulated significantly in both cases as expected from Figs. 4C and 5F, resulting in fluctuations in diverse metabolites (Fig. 6B). The size of the accumulated citrate pool was significantly larger than that of other organic acids in the TCA cycle (Fig. 6C). Because citrate originates from carbohydrate metabolism, we evaluated ^{13}C influx into the citrate pool 24 hours after administration of ^{13}C-labeled galactose. We found that a large amount of sugar-derived ^{13}C was incorporated into the citrate pool (Fig. 6D). On the basis of these results, we concluded that carbohydrate flux was largely directed to the citrate pool. The rewiring of carbohydrate pools likely affects the production of other metabolites derived from sugar because cytosolic citrate synthesis perturbs normal carbon flux through which hexose is oxidized and eventually converted into CO_2 in the mitochondria. Pathway analysis revealed that many amino acids and nucleotide metabolic pathways were affected in addition to the TCA and glyoxylate cycles, both of which include citrate as a component (Fig. 6E and fig. S6, A and B). Intriguingly, a marked decrease in aspartate and an increase in glutamine and glutamate were observed in both WT cells accumulating NΔCit1 and *tom40-97* cells accumulating preCit1 (Fig. 6F). Because these amino acids are used for de novo synthesis of nucleotides, the observed amino acid imbalance was predicted to affect nucleic acid metabolism, and nucleotide and deoxynucleotide levels did indeed decrease (Fig. 6G). However, the supplementation of nutrients outside of
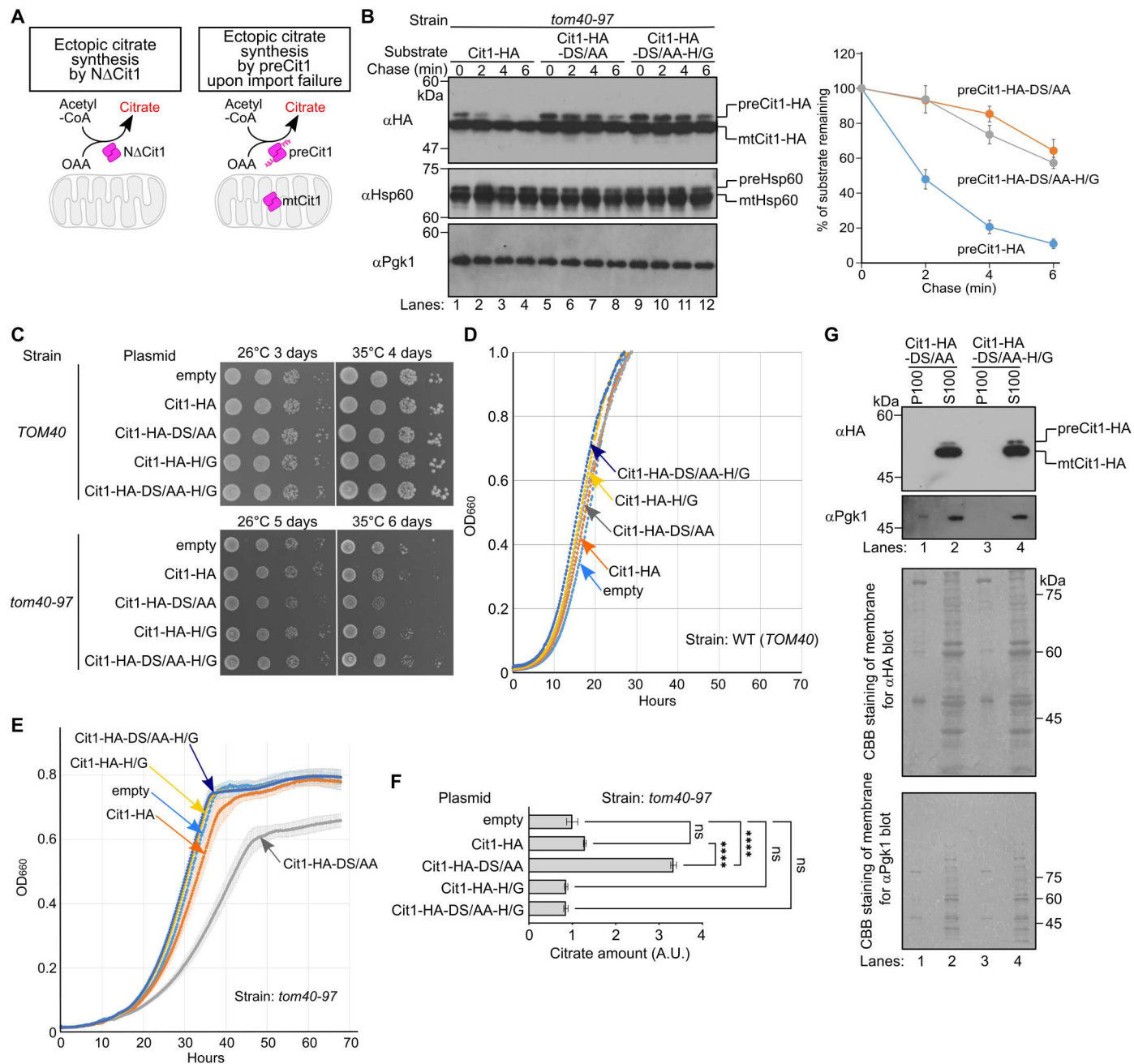
Fig. 5. Accumulation of preCit1 is toxic to cells in an enzymatic activity–dependent manner. (**A**) Schematic representation of ectopic citrate metabolism caused by NΔCit1 and preCit1. (**B**) Stabilities of preCit1-HA and its derivatives expressed under the control of the *GAL1* promoter were analyzed in *tom40-97* mutant cells by cycloheximide chase assay. Pgk1 served as a loading control. Results are means ± SE of three independent experiments. (**C**) Ten-fold serial dilutions of *TOM40* (JKR101) cells and *tom40-97* cells expressing Cit1-HA or its mutant derivatives were spotted on SGal medium. Cells were grown at 26° or 35°C for 3 to 6 days. (**D** and **E**) Growth rates of *TOM40* (JKR101) cells and *tom40-97* cells expressing Cit1-HA or its mutant derivatives. Cells were inoculated into SGal medium before the OD_{600} (optical density at 600 nm) was measured every 12 min. Results for *tom40-97* cells are means ± SE of five independent experiments. (**F**) Cellular citrate levels were measured in *tom40-97* cells expressing Cit1-HA and its mutant derivatives under the control of the *GAL1* promoter. Values are arbitrary units, and the amount of citrate in cells harboring empty vector was set to 1.0. Data represent the means ± SE of three independent experiments; ****$P < 0.0001$; ns, not significant; one-way ANOVA with Bonferroni's multiple comparison test. (**G**) Solubilities of preCit1 and mtCit1-HA-DS/AA or Cit1-HA-DS/AA-H/G overexpressed in *tom40-97* cells under the control of the *GAL1* promoter were analyzed by the ultracentrifugation at 100,000g for 1 hour at 4°C in the presence of 1% Triton X-100. The supernatant (S100) and pellet (P100) fractions were subjected to SDS-PAGE analysis. Blots for Pgk1 (soluble protein) and CBB staining of membranes are shown.
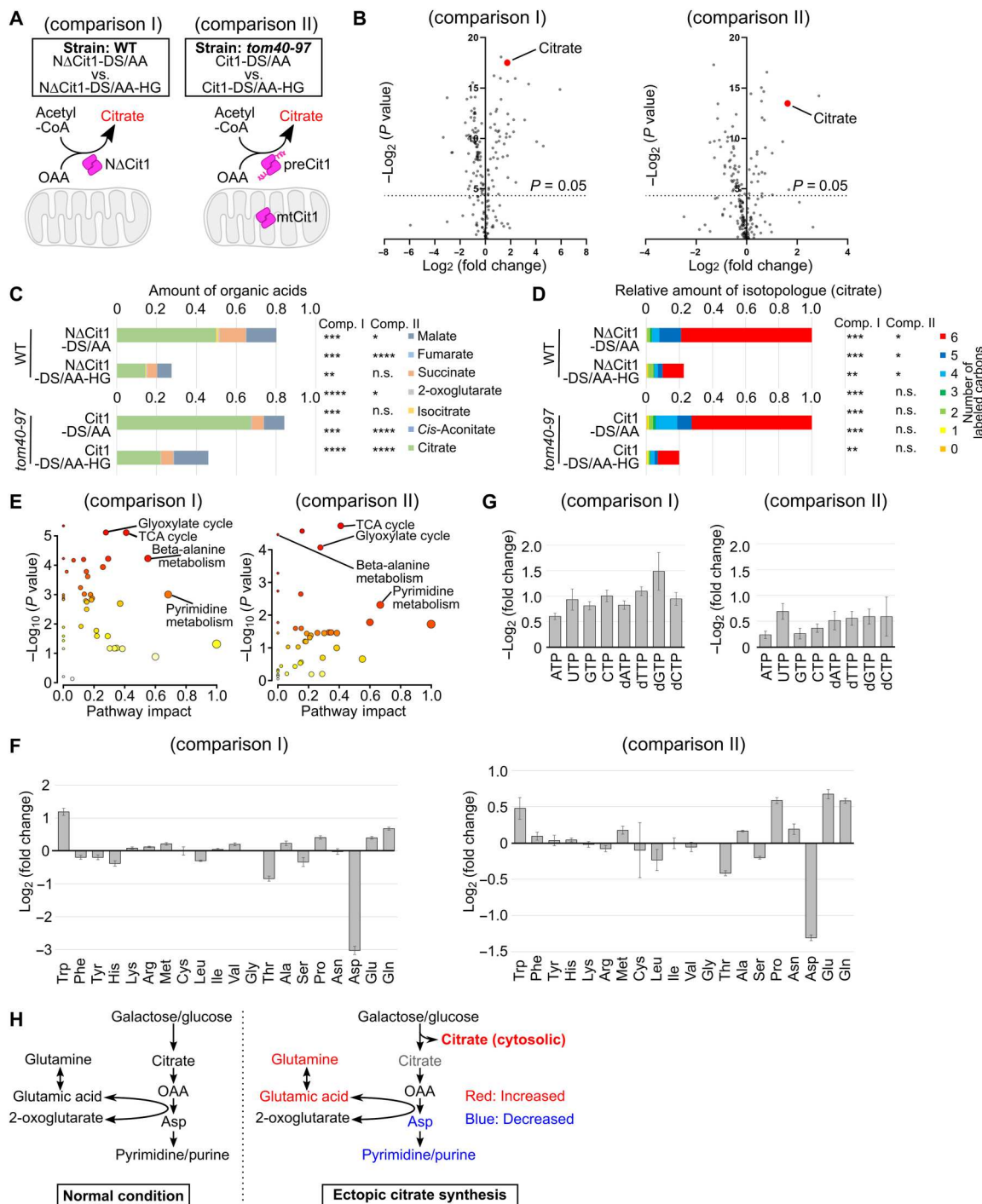
Fig. 6. Metabolome analysis of cells exhibiting ectopic citrate synthesis. (**A**) Schematic representation of the experimental design. Metabolomics profiles of WT cells expressing NΔCit1-DS/AA and NΔCit1-DS/AA-H/G (left, comparison I) and those of *tom40-97* cells expressing Cit1-DS/AA and Cit1-DS/AA-H/G (right, comparison II) were compared. (**B**) Volcano plots for 186 and 184 metabolites (comparison I and II, respectively) analyzed in this study. (**C**) Quantification of the levels of organic acids constituting the TCA cycle (peak areas normalized by external standards) in four yeast strains described in (A). Comp. I and II denote comparison I and II in (A), respectively. Results in graphs are means of three independent experiments; *$P < 0.05$, **$P < 0.01$, ***$P < 0.001$, and ****$P < 0.0001$; two-tailed unpaired t test. (**D**) Four yeast strains described in (A) were grown in the presence of ^{13}C-galactose as a sole carbon source for 24 hours before ^{13}C influx into the intracellular citrate pool was measured and expressed as relative amounts of isotopologue. Results in graphs represent means of three independent experiments; *$P < 0.05$, **$P < 0.01$, and ***$P < 0.001$, two-tailed unpaired t test. (**E**) Pathway enrichment analysis for comparisons I and II. (**F** and **G**) Changes in amino acid (F) and nucleotide and deoxynucleotide (G) levels in comparisons I or II represented as fold change. ATP, adenosine triphosphate; UTP, uridine triphosphate; GTP, guanosine triphosphate; CTP, cytidine triphosphate; dATP, deoxyadenosine triphosphate; dTTP, deoxythymidine triphosphate; dGTP, deoxyguanosine triphosphate; dCTP, deoxycytidine triphosphate. (**H**) Schematic representation of the consequence of ectopic citrate synthesis. Nucleotide metabolism was affected via amino acid metabolism in both comparisons I and II. n.s., not significant.

cells did not completely rescue the growth defect of cells expressing NΔCit1 (fig. S6C). Ectopic citrate synthesis likely causes decreases and increases of different kinds of metabolites and disrupts the global metabolic balance.

Nonetheless, intracytosolic retention of citrate seems to attenuate sugar-based aspartate production (via OAA production in the mitochondrial TCA cycle), and aspartate deficiency may have impaired nucleotide production. By contrast, levels of glutamate and glutamine, which donate amino groups to OAA in this pathway, were elevated, supporting this interpretation. Thus, cytosolic citrate synthesis may cause an amino acid imbalance and a decrease in purine/pyrimidine nucleotides via a shift in carbon flux from sugar (Fig. 6H).

Translation repression mitigates growth defect from mislocalized citrate turnover

To more broadly investigate the cellular response against ectopic citrate synthesis, we performed a transcriptome analysis of cells expressing NΔCit1-DS/AA or NΔCit1-DS/AA-H/G. Next-generation RNA sequencing revealed that citrate synthesis in the cytosol altered the levels of transcripts encoding >2600 genes (fig. S7A). Notably, up-regulated mRNAs included the targets of stress-responsive Msn2/Msn4 transcription factors, which also control the energy metabolism (17, 52, 53). msn2Δ cells and msn4Δ cells were sensitive to the expression of NΔCit1-DS/AA but not NΔCit1-DS/AA-H/G (fig. S7B), suggesting that the Msn2/Msn3-mediated stress response protects cells from the metabolic perturbation by cytosolic citrate synthesis. By contrast, mRNAs encoding translation, ribosome biogenesis, ribosomal RNA processing, and ribosome assembly were down-regulated significantly (Fig. 7A and fig. S7C). Therefore, we performed a puromycin incorporation assay to directly evaluate translation efficiency. Puromycin is a chain terminator that is incorporated into growing nascent polypeptide chains and can be detected by Western blotting (WB) using an anti-puromycin antibody (54). The efficiency of puromycin incorporation in cells expressing NΔCit1-DS/AA (Fig. 7B, lane 2) was lower than that in cells expressing NΔCit1-DS/AA-H/G (lane 4). Pretreatment of cells with cycloheximide blocked puromycin incorporation (lanes 1 and 3), confirming the detection of newly synthesized proteins. This result suggested that cytosolic citrate synthesis decreases translation efficiency. To confirm this finding, we also performed a polysome fractionation assay, in which the relative amounts of monosomes and polysomes are detected. We found that the relative monosome:polysome fraction was higher in cells expressing NΔCit1-DS/AA than in those expressing NΔCit1-DS/AA-H/G (Fig. 7C).

Last, we examined whether translation repression plays a protective role in alleviating cellular dysfunction. To this end, we deleted the DOT6 and TOD6 genes, whose products have partially overlapping functions, to repress the expression of ribosome biogenesis genes downstream of the target of rapamycin complex 1 and cyclic adenosine 3′,5′-monophosphate–dependent protein kinase pathways (55–57). As shown in Fig. 7D, the overexpression of NΔCit1-DS/AA slowed the growth of WT cells, as observed earlier, as well as that of dot6Δ cells and tod6Δ cells (Fig. 4B; galactose plate, WT, dot6Δ, and tod6Δ). The growth defect was exaggerated when DOT6 and TOD6 were simultaneously deleted (dot6Δtod6Δ). In contrast, cellular growth was unaffected even in dot6Δtod6Δ cells when NΔCit1-DS/AA with the H/G mutation was expressed. A similar trend was observed when the growth

phenotype was analyzed in liquid medium (Fig. 7E). These results suggest that translation repression protects against ectopic citrate synthesis.

DISCUSSION

While the quality control pathways for nonimported mitochondrial proteins have been extensively studied in recent years, it remains largely unclear how these proteins are recognized for degradation, how cells respond to their accumulation, and how their excess accumulation causes cell dysfunction. In this study, we demonstrate that, in contrast to the assumption that precursor proteins are kept in an unfolded, import-competent state in the cytosol, nonimported citrate synthase almost certainly forms an enzymatically active conformation, which is recognized and degraded by the ubiquitin ligase SCF^{Ucc1} and the proteasome. Defects in its degradation and its excess accumulation led to abnormal production of citrate in the cytosol, amino acid imbalances, purine/pyrimidine nucleotide depletion, and a cellular growth defect. Under these conditions, we found that translation repression was induced and acted as a protective mechanism for cell survival. On the basis of these results, we propose that mitochondrial import failure not only causes a proteotoxic insult but also triggers ectopic metabolic stress (Fig. 7F).

Ucc1 was originally identified as a factor that targets cytosolic citrate synthase Cit2 for proteasomal degradation to regulate the activity of glyoxylate cycle. Our structural study of Skp1-Ucc1-Cit2 revealed that Ucc1 preferentially recognized the ligand-free form but not the ligand-bound form of citrate synthase. Moreover, in contrast to the canonical degron-based substrate recognition, it turned out that Ucc1 discriminates relatively subtle but refined structural change caused by binding of acetyl-CoA and OAA during the physiological catalytic cycle of citrate synthase. These results provide a structural basis for our previous observation that Cit2 is stabilized more in cells where there is a higher amount of gluconeogenic metabolites (e.g., acetyl-CoA and OAA) to further activate the glyoxylate cycle (34). Our structural study also suggested that Ucc1 recognizes the folded citrate synthase rather than the peptide motif. In addition, Ucc1 targeted preCit1 for proteasomal degradation. These findings inspired us to investigate the possible enzymatic activities of nonimported Cit1 and the cellular consequences of its accumulation.

The amount of TCA cycle metabolites in the cytosol has been shown to be crucial for epigenetic regulation, the regulation of transcription factors such as hypoxia-inducible factor-1α, and the regulation of pluripotency (58, 59). While ectopically localized excess metabolites generated upon mitochondrial import failure could cause cellular stress, they could also function similar to a "second messenger" that cooperatively transmits the mitochondrial status to the nucleus and other cellular components. Further investigation is needed to clarify whether a broad range of metabolic enzymes or a specific subset of them are active outside mitochondria upon import failure. In either case, we speculate that mitochondrial import deficiency would generate a broad spectrum of ectopic metabolites, and their constituents may differ depending on mitochondrial status. In this respect, we propose that the ectopic citrate synthesis analyzed in this study can be considered as a "model metabolic perturbation." One potential downstream event could be the ISR activation through eukaryotic initiation factor 2 alpha subunit (eIF2α) (Sui2 in yeast) phosphorylation (60); however, we failed to
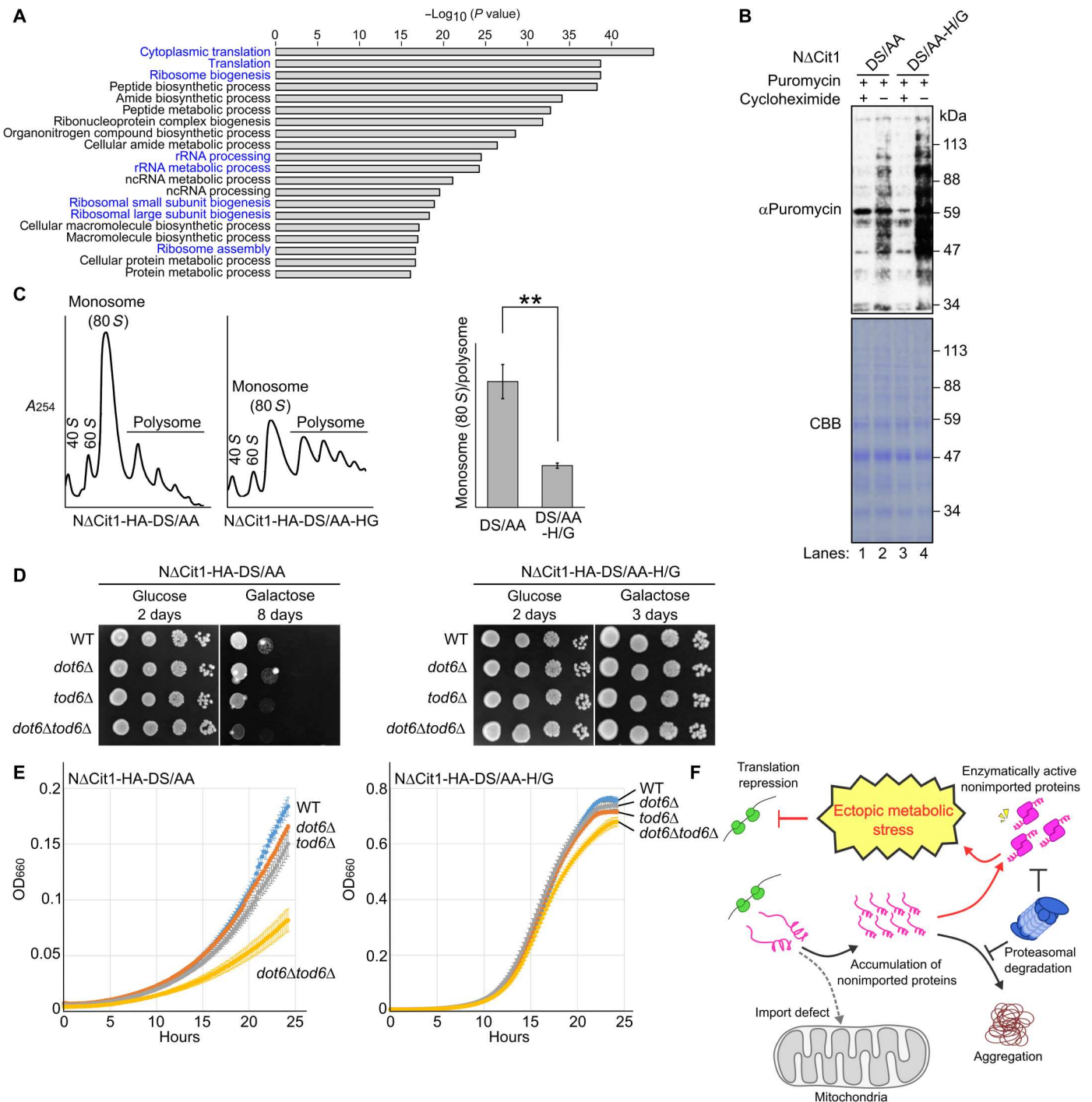
Fig. 7. Translation repression protects cells during ectopic citrate stress. (**A**) Top 20 Gene Ontology biological processes that were down-regulated at the transcriptional level in cells expressing NΔCit1-HA-DS/AA compared with cells expressing NΔCit1-HA-DS/AA-H/G. rRNA, ribosomal RNA; ncRNA, noncoding RNA. (**B**) Cells expressing NΔCit1-HA-DS/AA or NΔCit1-HA-DS/AA-H/G were treated with puromycin (200 μg/ml) for 20 min. Whole-cell lysates were analyzed by WB with an anti-puromycin antibody. Where indicated, cells were treated with cycloheximide (100 μg/ml) for 5 min before puromycin. CBB staining of the SDS-PAGE gel served as a loading control. (**C**) Polysome profiles of cells expressing NΔCit1-HA-DS/AA or NΔCit1-HA-DS/AA-H/G. The monosome (80S)/polysome ratio was calculated on the basis of the trapezoidal area under the curve. Data in the graphs represent the means ± SE of four independent experiments; A_{254}, UV absorbance at 254 nm; **$P < 0.01$, two-tailed unpaired t test. (**D**) Ten-fold serial dilutions of WT, $dot6\Delta$, $tod6\Delta$, and $dot6\Delta tod6\Delta$ cells expressing NΔCit1-HA-DS/AA or NΔCit1-HA-DS/AA-H/G under the control of the *GAL1* promoter were spotted on SD (glucose) or SGal (galactose) medium. Cells were grown at 30°C for 2 to 8 days. (**E**) Growth rates of WT, $dot6\Delta$, $tod6\Delta$, and $dot6\Delta tod6\Delta$ cells expressing NΔCit1-HA-DS/AA or NΔCit1-HA-DS/AA-H/G were measured in SGal medium. Data represent the means ± SE of five independent experiments. (**F**) Model depicting the ectopic metabolic stress response. See text for details.

observe eIF2α-P (fig. S7D). Instead, we found that the Dot6/Tod6-mediated repression of ribosome biogenesis and the Msn2/Msn4-mediated stress response were involved in the downstream events of ectopic citrate stress (Fig. 7 and fig. S7).

The importance of regulating intracellular citrate concentrations is underscored by the fact that citrate is involved in inflammation, cancer, insulin secretion, histone acetylation, neurological disorders, and several metabolic diseases (61, 62). In addition, citrate levels are high in patients with nonalcoholic fatty liver disease (NAFLD) and in those with citrin deficiency, which is caused by a rare genetic defect that causes a dysfunctional mitochondrial aspartate/glutamate carrier (61). The mechanism by which citrate causes these diseases is still enigmatic, but recent studies suggest that citric acid triggers the mitochondrial unfolded protein response (UPR^{mt}) in *Caenorhabditis elegans* (63). Our finding that cytosolic accumulation of citrate causes a metabolic imbalance (e.g., amino acid and nucleotide pools) and translational repression may provide potential insights into these diseases.

Several important questions remain unanswered. It is now possible that precursors of mitochondrial metabolic enzymes, which were assumed to be in an unfolded, import-competent state in the cytosol, could achieve a catalytically active conformation outside of the mitochondria. However, it remains unclear whether their folding occurs during the normal import process before they are docked onto the import receptor at the TOM or whether it is only facilitated when they remain in the cytosol for a prolonged period as a result of an import deficiency. Second, the potential mechanisms by which cytosolic chaperones and other factors contribute to the discrimination between import, degradation, and folding of newly synthesized mitochondrial precursor proteins in vivo require clarification. Moreover, it will be important to elucidate the physiological significance of why only a limited number of substrates are degraded. Third, although Ucc1 is only conserved in fungal species (64), our results demonstrate that it is a critical F-box protein that controls citrate metabolism. In this respect, it should be noted that in mammals, Ubr5-mediated ubiquitination and degradation was suggested to regulate the level of citrate synthase in triple-negative breast cancer cells (65). Fourth, it remains to be established whether ectopic metabolic stress represses the translation of global proteins or a specific subset of proteins. It is also important to analyze the time frame, namely, whether the translation repression happens once a specific change in metabolic products occurs. Last, changes in mitochondrial import rates have been shown to affect the longevity of nematodes (66). Thus, analyzing the contribution of ectopic metabolism to these events represents a future line of work.

Clearly, the precise localization of metabolites is a fundamental aspect of cellular homeostasis, and their mislocalization can lead to functional decline and cellular deficiencies. The technical advancement of methods that can detect the quantity and localization of cellular metabolites would deepen our understanding of the ectopic metabolic stress and may aid the development of future pharmacological and engineering approaches to neurodegenerative disease, cancer, cellular differentiation, development, and aging.

MATERIALS AND METHODS
Yeast strains and plasmids
The yeast strains used in this study are listed in the table S1. Plasmids used in this study are listed in the table S2. Yeast strains were grown in YP-rich medium [1% yeast extract, 1% peptone, and adenine hydrochloride (100 mg/liter)] containing 2% glucose (YPD), 2% galactose (YPGal), or synthetic complete medium [0.67% yeast nitrogen base without amino acids, adenine hydrochloride (100 mg/liter), and all standard amino acids] containing 2% glucose (SD), 2% raffinose (SRaf), or 2% galactose (SGal). Where indicated, cells were grown in synthetic minimum medium [0.67% yeast nitrogen base without amino acids and adenine hydrochloride (100 mg/liter)] containing only necessary amino acids and 2% carbon source.

Protein expression and purification
Ucc1-Skp1 expression
DNA fragments encoding HisSUMO1-Ucc1 or its mutant derivatives, Skp1(FL), or Skp1(ΔL) were cloned into a pET21 vector. The resultant plasmids were transformed into BL21(DE3) cells. The transformants were inoculated into LB medium containing ampicillin (100 μg/ml) and were cultured at 37°C until the OD$_{600}$ (optical density at 600 nm) reached ~0.5. Protein expression was induced by the addition of 0.1 mM isopropyl-β-ᴅ-thiogalactopyranoside (IPTG) and incubation at 18°C overnight. Cells were pelleted and stored at −80°C until purification.

Cit2 expression
To express HisSUMO1-tagged Cit2, the DNA fragment encoding WT Cit2 with an N-terminal HisSUMO1-tag was cloned into the pET28 vector. The resultant plasmid, pET28-HisSUMO1-Cit2, was transformed into BL21(DE3) cells. The cells were inoculated into LB medium containing kanamycin (20 μg/ml) and were cultured at 37°C until the OD$_{600}$ reached 0.5. Protein expression was induced by the addition of 0.1 mM IPTG and incubation at 18°C overnight. Cells were pelleted and stored at −80°C until purification. To express N-terminally MBP-tagged Cit2, DNA fragments encoding WT and mutant derivatives of Cit2 were cloned into the pMAL-p2X (New England Biolabs) vector. The series of pMAL-Cit2 plasmids encoding WT Cit2 or its mutant derivatives (D154A, E309A, R332A, or S409A/S410A) were transformed into BL21(DE3) cells. The transformants were inoculated in LB medium containing ampicillin (100 μg/ml) and were cultured at 37°C until the OD$_{600}$ reached 0.5. Protein expression was induced by the addition of 0.1 mM IPTG and incubation at 18°C overnight. Cells were pelleted and stored at −80°C until purification.

Cit1 expression
To express HisSUMO1-tagged Cit1(Δ1−37), the DNA fragment encoding WT Cit1 that lacked the N-terminal mitochondrial signal sequence (residues 1 to 37) was fused to an N-terminal HisSUMO1-tag. The resultant fragment, HisSUMO1-Cit1(Δ1−37), was cloned into a pCold vector. The resultant plasmid, pCold-HisSUMO1-Cit1(Δ1−37), was transformed into BL21(DE3) cells. The transformant was inoculated into LB medium containing ampicillin (100 μg/ml) and was cultured at 37°C until the OD$_{600}$ reached 0.5. Protein expression was induced by the addition of 0.1 mM IPTG and incubation at 18°C overnight. Cells were pelleted and stored at −80°C until purification. To express N-terminally MBP-tagged Cit1(Δ1−37), the DNA fragment encoding Cit1(Δ1−

37) was cloned into a pMAL vector. The resultant plasmid, pMAL-Cit1(Δ1−37), was transformed into BL21(DE3) cells. The transformant was inoculated in LB medium containing ampicillin (100 µg/ml) and was cultured at 37°C until the OD_{600} reached 0.5. Protein expression was induced by the addition of 0.1 mM IPTG and incubation at 18°C overnight. Cells were pelleted and stored at −80°C until purification.

Cit2-Ucc1-Skp1 complex expression

To express the Cit2-Ucc1-Skp1 complex, pET21-ySkp1-HisSUMO1-Ucc1 and pET28-HisSUMO1-Cit2 were simultaneously transformed into BL21(DE3) cells. The transformant was inoculated in LB medium containing ampicillin (100 µg/ml) and kanamycin (20 µg/ml) and was cultured at 37°C until the OD_{600} reached 0.5. Protein coexpression was induced by the addition of 0.1 mM IPTG and incubation at 18°C overnight. Cells were pelleted and stored at −80°C until purification.

Purification of the Cit2-Ucc1-Skp1 complex

To purify the Cit2-Ucc1-Skp1 complex for crystallization, frozen cell pellets were thawed and resuspended in lysis buffer [20 mM tris-HCl (pH 7.5) and 150 mM NaCl]. Subsequently, the cells were lysed by sonication, and cell debris was removed by centrifugation. The supernatant was subjected to purification using Ni-NTA resin (Ni Sepharose 6 FF, GE HealthCare) affinity column chromatography. Unbound proteins were washed away using Ni-NTA column washing buffer [20 mM tris-HCl (pH 7.5), 20 mM imidazole, and 500 mM NaCl], and then the bound protein was eluted from the column using Ni-NTA column elution buffer [20 mM tris-HCl (pH 7.5), 300 mM imidazole, and 500 mM NaCl]. The eluates were dialyzed overnight at 4°C against dialysis buffer [25 mM tris-HCl (pH 7.5) and 10 mM β-mercaptoethanol]. The HisSUMO1-tag was cleaved from the complex by treatment with a HisSUMO1-tagged Ulp1 protease (in-house) after dialysis. To separate the cleaved HisSUMO1-tag from the Cit2-Ucc1-Skp1 complex, proteins were purified by size exclusion column chromatography (HiLoad 26/600 Superdex 200 pg, GE HealthCare) using a fast protein LC (FPLC) system (AKTA explore, GE HealthCare). The column was equilibrated and eluted with size exclusion column buffer A [25 mM tris-HCl (pH 7.5), 150 mM NaCl, and 10 mM β-mercaptoethanol]. The eluates were dialyzed overnight at 4°C against crystallization buffer [25 mM tris-HCl (pH 7.5) and 1 mM dithiothreitol (DTT)] and then concentrated to ~15 mg/ml using a centrifugal concentrator (Amicon Ultra, Merck).

Purification of Cit1 and Cit2

To purify Cit1 and Cit2 for crystallization, frozen cell pellets were thawed and resuspended in lysis buffer. Subsequently, the cells were lysed by sonication, and cell debris was removed by centrifugation. The supernatant was subjected to purification using Ni-NTA resin affinity column chromatography. Unbound proteins were washed away using Ni-NTA column washing buffer, and then the bound protein was eluted from the column using Ni-NTA column elution buffer. The eluates were dialyzed overnight at 4°C against dialysis buffer. The HisSUMO1-tag was cleaved from Cit1 or Cit2 by treatment with a HisSUMO1-tagged Ulp1 protease (in-house) after dialysis. To separate the cleaved HisSUMO1-tag from Cit1 or Cit2, proteins were purified by size exclusion column chromatography (HiLoad 26/600 Superdex 75 pg, GE HealthCare) using an FPLC system. The column was equilibrated and eluted with size exclusion column buffer A. The eluates were dialyzed overnight at 4°C against crystallization buffer and then concentrated to ~25 mg/ml using a centrifugal concentrator.

Purification of the MBP-Cit1 and -Cit2 series

To purify MBP-Cit1 and MBP-Cit2 for assay, frozen cell pellets were thawed and resuspended in lysis buffer. Subsequently, the cells were lysed by sonication, and cell debris was removed by centrifugation. The supernatant was subjected to amylose resin affinity column chromatography (Amylose resin, NEB). Unbound proteins were washed away using lysis buffer, and then the bound protein was eluted from the column using amylose column elution buffer [20 mM tris-HCl (pH 7.5), 150 mM NaCl, and 10 mM maltose]. Proteins were purified further by size exclusion column chromatography (HiLoad 26/600 Superdex 200 pg, GE HealthCare) using an FPLC system. The column was equilibrated and eluted with size exclusion column buffer A. The eluates were dialyzed overnight at 4°C against dialysis buffer and then concentrated to ~3 mg/ml using a centrifugal concentrator.

Purification of the Ucc1-Skp1(FL) series

To purify the Ucc1-Skp1(FL) series for assay, frozen cell pellets were thawed and resuspended in lysis buffer. Subsequently, the cells were lysed by sonication, and cell debris was removed by centrifugation. The supernatant was subjected to Ni-NTA resin affinity column chromatography. Unbound proteins were washed out with Ni-NTA column washing buffer, and then the bound protein was eluted from the column using Ni-NTA column elution buffer. The eluates were dialyzed overnight at 4°C against size exclusion column buffer B [40 mM tris (pH 7.5), 60 mM NaCl, and 10% glycerol]. The HisSUMO1-tag was cleaved from the complex by treatment with a HisSUMO1-tagged Ulp1 protease (in-house) after dialysis. To separate the cleaved HisSUMO1-tag and the Ucc1-Skp1 complex, proteins were subjected to size exclusion column chromatography (HiLoad 16/600 Superdex 75 pg, GE HealthCare) using an FPLC system. The column was equilibrated and eluted with size exclusion column buffer B. The eluates were dialyzed overnight at 4°C against dialysis buffer and then concentrated to ~5 mg/ml using a centrifugal concentrator.

Structure determination of Cit1 and Cit2

Crystallization experiments were performed by sitting-drop vapor diffusion at 20°C. A 1-µl aliquot of protein sample was mixed with 1 µl of reservoir solution. For Cit2-OAA-CoA sample preparation, Cit2 was mixed with 20 mM OAA and 20 mM CoA and then incubated at 4°C for 1 hour. Crystals of Apo-Cit1 were obtained from a Cit1 sample mixed with reservoir solution [140 mM $Ca(OAc)_2$, 70 mM tris (pH 7.0), and 14% (w/v) PEG-3000 (polyethylene glycol, molecular weight 3000)]. Crystals of Apo-Cit2 were obtained from a Cit2 sample mixed with reservoir solution [90 mM KCl, 90 mM Hepes (pH 7.5), 13.5% (w/v) PEG-6000]. Crystals of Cit2-OAA-CoA were obtained from a Cit2-OAA-CoA sample mixed with reservoir solution [80 mM KCl, 80 mM Hepes (pH 7.5), and 12% (w/v) PEG-6000]. Crystals were soaked in the reservoir solution containing 20% glycerol and were flash frozen in liquid nitrogen. Diffraction data were collected at 100 K on beamline BL44XU at the SPring-8 facility, with a wavelength of 0.9000 Å, using an MX-300HE charge-coupled device (CCD) detector (Rayonix). The datasets were processed using HKL-2000 software (67). Data collection and processing statistics for the crystals are given in table S3. The structure of Apo-Cit2 was solved by molecular replacement (MR) using Phaser (68) with the Cit2 homology model. The Cit2 homology model for MR was generated using

the pig citrate synthase structure (Protein Data Bank code: 1CTS), whose sequence was substituted with Cit2 using the SWISS-MODEL server (69). The Apo-Cit2 model was built using COOT (70) and was refined using PHENIX (71). The structures of Apo-Cit1 and Cit2-OAA-CoA were also determined by MR.

Structure determination of Cit2-Ucc1-Skp1

Crystallization experiments were performed by sitting-drop vapor diffusion at 20°C. A 1-μl aliquot of protein sample was mixed with 1 μl of reservoir solution. Crystals of the Cit2-Ucc1-Skp1(FL) complex were obtained from a Cit2-Ucc1-Skp1(FL) sample mixed with reservoir solution [200 mM Na acetate, 100 mM Na citrate (pH 5.5), and 10% (w/v) PEG-4000]. Crystals of the Cit2-Ucc1-Skp1(ΔN) complex were obtained from a Cit2-Ucc1-Skp1(ΔN) sample mixed with reservoir solution [70 mM Na citrate (pH 5.5) and 10.5% (w/v) PEG-6000]. Cit2-Ucc1-Skp1(FL) and Cit2-Ucc1-Skp1(ΔL) crystals were soaked in reservoir solution containing 20% glycerol and 20% ethylene glycol, respectively, and then flash frozen in liquid nitrogen. Diffraction data were collected at 100 K on beamline BL44XU at the SPring-8 facility, with a wavelength of 0.9000 Å, using an MX-300HE CCD detector. The datasets were processed using HKL-2000. Data collection and processing statistics for the crystals are given in table S3. The initial phases of Cit2-Ucc1-Skp1(FL) were calculated by MR using Phaser with the Cit2 homology model as a search model. The initial model was automatically built using Buccaneer (72), and the manual model was built using COOT, with structural refinement using PHENIX. The extra electron density was interpreted for Ucc1 and Skp1(FL), whereas the N-terminal region of Skp1 was disordered. The structure of Cit2-Ucc1-Skp1(ΔL) was determined using the refined model of Cit2-Ucc1-Skp1(FL). The density quality of the N-terminal region of Skp1(ΔL) was slightly higher than that of Skp1(FL). Protein structures and electrostatic surfaces were visualized with PyMOL (www.pymol.org). The Cit2-Ucc1 interactions were analyzed using LigPlot+ (73). The protein domain motion was analyzed using DynDom (74).

Cycloheximide chase experiment

The cycloheximide chase protein degradation assay was performed as described previously (34). In Fig. 2 (E to G) and fig. S5 (A and E), NΔCit1-HA, Cit1-HA, or their mutant derivatives were expressed under the control the CIT1 promoter from a low-copy plasmid. In Figs. 3D and 5B, the expression of NΔCit1-HA, Cit1-HA, or their mutant derivatives was induced under the GAL1 promoter from a low-copy plasmid for 30 min and 2 hours, respectively. Cit2-GFP-SKL was expressed from its endogenous locus under the control of its own promoter (fig. S1D). In fig. S5A, tom40-97 cells harboring a low-copy plasmid encoding Cit1-HA or Cit1-HA-DS/AA under the control of the CIT1 promoter were grown in SGal medium until OD_600 reached 0.5 to 1.2. Cit1 expressed from its endogenous locus from its own promoter was observed in fig. S5F. To allow the action of the proteasome inhibitor (MG132), a pdr5Δ null mutant was used in Fig. 2E . To assess the stability of NΔCit1-HA in the SCF temperature-sensitive strains (Fig. 2F), cells were grown at 26°C and shifted to 30°C for 3 hours before cycloheximide was added. When the stability of preCit1-HA was analyzed in cells expressing b2(220)-DHFR (fig. S5E), the cells were first grown in SD medium and then diluted ~100-fold into YPGal medium to induce b2(220)-DHFR expression for 16 hours at 30°C. When the stability of endogenous preCit1 was

analyzed in cells expressing b2(220)-DHFR (fig. S5F), cells were first grown in YPD medium and then diluted ~100-fold into YPGal medium to induce b2(220)-DHFR expression for 16 hours at 30°C. When the stability of preCit1-HA was analyzed in tom40-97 cells (Fig. 5B), cells were grown in SRaf medium to OD_600 = 1.0 to 2.0, and then the Cit1 expression was induced by adding 2% galactose for 2 hours before cycloheximide was added to the culture. In all methods, cycloheximide was added at a final concentration of 100 to 200 μg/ml. At the indicated time points, cells were collected and suspended in 20% trichloroacetic acid on ice. The cells were then collected by centrifugation, and the pellet was stored at −30°C. Subsequently, the cell pellet was suspended in 300 μl of 20% trichloroacetic acid and lysed by vigorous vortexing with glass beads for ~30 min (TAITEC Max Mixer EVR-032), with occasional inversion of the tube to prevent the accumulation of cells at the bottom. The broken cell lysate was added to 900 μl of 5% trichloroacetic acid, the tube was inverted several times, and then 900 μl of the suspension was transferred to a new tube. Proteins were precipitated by centrifugation at 20,000g for 15 min at 4°C. The precipitates were dissolved in either KNTCASB [80 mM tris-HCl (pH 7.5), 8 mM EDTA (pH 8.0), 12.5% glycerol, 8 M urea, 4% SDS, 200 mM DTT, tris (0.8 mg/ml), and 0.1% Bromophenol blue (BPB)]. Before SDS–polyacrylamide gel electrophoresis (SDS-PAGE) and WB analyses, samples were heated at 55°C for 15 min and cleared by centrifugation at 20,000g for 1 min at room temperature.

Immunoblotting

Proteins were transferred from polyacrylamide gels to Immobilon-P membranes (Millipore) in blotting buffer (25 mM tris, 192 mM glycine, and 10% methanol) using the GENIE electrophoretic transfer device (Idea Scientific Company) at a constant current of 650 mA. The membranes were washed with TBS-T buffer [20 mM tris-HCl (pH 7.5), 150 mM NaCl, and 0.1% Tween 20) and, when necessary, blocked with 3% skimmed milk in TBS-T buffer for 30 min. Subsequently, the membranes were incubated with primary antibodies in either TBS-T buffer or TBS-T buffer supplemented with 3% skimmed milk at 4°C overnight. The membranes were then washed three times with TBS-T (10 to 60 min per wash), incubated with secondary antibodies for ~60 min, and washed three times with TBS-T. Last, the membranes were incubated with Chemi-Lumi One (Nacalai Tesque) or Luminata Forte Western HRP substrate (Millipore) and exposed to x-ray film. Band intensities were quantified with ImageJ [National Institutes of Health (NIH)] directly from films scanned at high resolution (EPSON, catalog no. GT-X980) in TIF file format (600 dpi). Anti-Pgk1 antibody was purchased from Abcam (#ab113687, 22C5D8). Anti-Cdc48 and anti-Hsp60 antibodies were gifts from T. Endo.

Fluorescence microscopy

Cells expressing Pgk1-mCherry from its endogenous locus and Cit1-EGFP or NΔCit1-EGFP under the control of the CIT1 promoter from a low-copy plasmid were inoculated into SGal medium and grown at 30°C. Cells were observed under an Axio Observer inverted microscope equipped with an Axiocam 503 mono camera (Carl Zeiss) manipulated by ZEN software. GFP was excited at 475 nm (Colibri 7 Type RYB-UV), and the emission was passed through a 524/50-nm band-pass filter {92 HE light-emitting diode (LED) [4′,6-diamidino-2-phenylindole (DAPI)/GFP/mCherry)]}; mCherry was excited at 590 nm (Colibri 7 Type RYB-UV), and

the emission was passed through a 688/145-nm band-pass filter [92 HE LED (DAPI/GFP/mCherry)].

Subcellular fractionation assay

Cells expressing NΔCit1-HA under the control of the *CIT1* promoter were grown in SGal medium until OD_{600} reached ~0.6. Cells (~300 OD_{600} equivalent) were collected by centrifugation and incubated with 10 ml of 100 mM tris-HCl (pH 9.4) supplemented with 10 mM DTT at 30°C for 10 min. Cells were collected again and suspended in 10 ml of KCl-EM buffer [180 mM KCl, 1 mM EDTA, and 5 mM Mops/KOH (pH 7.2)] supplemented with 2.5 mg of Zymolyase-100 T (Nacalai Tesque, catalog no. 07665-55) and incubated at room temperature for 30 min. Cells were chilled on ice, collected by centrifugation, and washed twice with ice-cold KCl-EM buffer. Cells were suspended in 4 ml of KCl-EM buffer supplemented with 1× complete EDTA-free protease inhibitor cocktail (PIC) (Roche, catalog no. 11873580001) and disrupted with a dounce homogenizer. The homogenate was centrifuged at 250*g* for 2 min, 1000*g* for 4 min, and 1900*g* for 4 min. The supernatant was transferred to a new tube and further centrifuged at 17,000*g* for 15 min at 4°C. The supernatant was saved as a cytosol fraction (S17). The resultant pellet was washed with KCl-EM and centrifuged again at 17,000*g* for 15 min at 4°C. The resultant pellet was saved as a membrane fraction (P17).

In vivo ubiquitination assay

Cells expressing Cit1-HA, NΔCit1-HA, or their mutant derivatives under the control of the *CIT1* promoter from a low-copy plasmid were transformed with the pKN365 plasmid (*2* μm, *TRP1*, P_{CUP1}-8xHis–tagged Ub). The cells were then cultured in SD medium overnight and diluted 50- to 100-fold in fresh medium. His-tagged ubiquitin expression was induced by adding 100 μM $CuSO_4$ to the medium for 5 to 8 hours before ~50 OD_{600} equivalents of cells were collected and stored at −80°C. Subsequently, the cells were lysed in 250 μl of buffer [20 mM tris-HCl (pH 7.5), 150 mM NaCl, 0.5% Triton X-100, 0.1% SDS, and 10 mM *N*-ethylmaleimide] supplemented with 1× PIC using glass beads in a round-bottom plastic tube by eight rounds of vigorous vortexing for 30 s with 30-s interval on ice. The same buffer (500 μl) was then added, and the suspension was transferred to a new tube. The glass beads were washed again with 500 μl of buffer and pooled in the same tube. The collected lysates were cleared by centrifugation at 15,000 rpm for 10 min at 4°C, and the cleared lysates were incubated with 1 μl of anti-HA antibody (MBL, catalog no. 180-3 TANA2) and Dynabeads Protein G (Invitrogen) at 4°C overnight. The beads were then washed four times with a buffer [20 mM tris-HCl (pH 7.5), 150 mM NaCl, 0.5% Triton X-100, 0.05% SDS, and 10 mM *N*-ethylmaleimide]. Immunoprecipitated proteins were eluted with KNTCASB at 55°C for 30 min, separated by SDS-PAGE, and subjected to WB. The extent of the polyubiquitin chains was detected with mono- and polyubiquitinated conjugated/mouse monoclonal antibody horseradish peroxidase conjugate (FK2H) (BioMol, #PW0150).

Pull-down analysis

The His_6-3xFLAG-Ucc1-Skp1 complex was purified from Sf21 cells that had been infected with a baculovirus encoding His_6-3xFLAG-Ucc1 and Skp1 by Ni-NTA agarose (FUJIFILM Wako, catalog no. 141-09764) chromatography (*34*). This complex was dialyzed against dialysis buffer [40 mM tris-HCl (pH 7.5), 60 mM NaCl,

and 10% glycerol] and stored at −80°C. The complex was then immobilized to anti-FLAG M2 affinity gel (Sigma-Aldrich) in a buffer [40 mM tris-HCl (pH 7.5), 150 mM NaCl, 10% glycerol, and 0.1% Triton X-100] by rotating at 4°C for ~30 min. Subsequently, the beads were washed three times with the same buffer. In parallel, *ucc1*Δ cells expressing Cit1-HA or NΔCit1-HA under the control of the *CIT1* promoter from a low-copy plasmid were lysed in buffer [40 mM tris-HCl (pH 7.5), 150 mM NaCl, and 0.5% Triton X-100] supplemented with 1× PIC using glass beads in a round-bottom plastic tube by eight rounds of vigorous vortexing for 30 s with 30-s intervals on ice. The suspension was added to 400 μl of the same buffer, and the suspension was transferred to a new tube. The glass beads were washed with 400 μl of buffer and pooled in the same tube. The lysates were cleared by centrifugation at 20,000*g* for 10 min at 4°C. A portion of the supernatant was saved, trichloroacetic acid–precipitated, dissolved in KNTCASB, and used as an input control. The remaining lysate was incubated with anti-FLAG beads that had been loaded with the His_6-3xFLAG-Ucc1-Skp1 complex (see above) and rotated at 4°C for 20 to 40 min. The beads were then washed five times with buffer [40 mM tris-HCl (pH 7.5), 150 mM NaCl, 10% glycerol, and 0.1% Triton X-100]. The proteins were eluted with KNTCASB at 55°C for 30 min, separated by SDS-PAGE, and subjected to WB.

For the in vitro pull-down assay with purified proteins, 25 μg of purified MBP-Cit2 and its mutant derivatives were incubated with 60 μl (50% slurry) of amylose resin, and the resin loaded with immobilized proteins was washed three times with 600 μl of pull-down buffer [40 mM tris-HCl (pH 7.5), 150 mM NaCl, and 10% glycerol]. The resulting immobilized MBP-Cit2 and its mutants were incubated with 16 μg of Ucc1-Skp1(FL) or its mutant derivatives at 4°C for 1 hour, washed three times, and then suspended in 20 μl of 2× Laemmli SDS-PAGE sample buffer. The resultant supernatants were subjected to SDS-PAGE, followed by Coomassie brilliant blue (CBB) staining.

Spot assay (serial dilution assay)

Spot assay was performed as described previously (*75*). Cells were transformed with a low-copy plasmid encoding Cit1-HA, NΔCit1-HA, or their mutant derivatives under the control of the *CIT1* promoter (fig. S4, B and E), a low-copy plasmid encoding Cit1-HA, NΔCit1-HA, or their mutant derivatives under the control of the *GAL1* promoter (Figs. 4, A and B; 5C; and 7D; and fig. S4A), a multicopy plasmid encoding Cit1-HA or NΔCit1-HA under the control of the *CIT1* promoter (fig. S4C) or a low-copy plasmid encoding Cit2-HA-SKL under the control of the *GAL1* promoter (fig. S4D).

Yeast growth analysis in liquid culture

In Fig. 5D, *TOM40* cells harboring a plasmid encoding Cit1 or its mutant derivatives under the control of the *GAL1* promoter were grown in SRaf medium at 30°C overnight and diluted 50-fold into SGal medium. In Fig. 5E, *tom40-97* cells harboring a plasmid encoding Cit1 or its mutant derivatives under the control of the *GAL1* promoter were grown in SRaf medium at 30°C until the OD_{600} reached 7.0 to 8.0. Cells were then diluted 50-fold into 1 ml of SGal medium to induce the expression of Cit1 or its mutant derivatives. In Fig. 7E, WT, *dot6*Δ, *tod6*Δ, or *dot6*Δ*tod6*Δ cells harboring a plasmid encoding NΔCit1-HA-DS/AA or NΔCit1-HA-DS/AA-H/G under the control of the *GAL1* promoter were grown in SRaf medium at 30°C and then diluted 200-fold into

SGal medium. In fig. S7B, WT, *msn2Δ*, or *msn4Δ* cells harboring a plasmid encoding NΔCit1-HA-DS/AA or NΔCit1-HA-DS/AA-H/G under the control of the *GAL1* promoter were grown in SRaf medium at 30°C and then diluted 200-fold into SGal medium. The cell culture was transferred to a 24-well plate (Cell Culture Plate TR5002 24 well, TrueLine), and the cell growth was analyzed at 30°C using a plate reader (Infinite 200 PRO, Tecan) that was set up to measure the OD_{660} at 10- or 12-min intervals. The plate was agitated for 15 to 45 s just before the optical density was measured. The initial value of OD_{660} was usually ~0.02. For each well, the OD_{660} was measured at four or nine positions, and the mean value was used for the analysis.

Citrate assay
In Fig. 4C and fig. S4F, cells expressing Cit1-HA, NΔCit1-HA, or their mutant derivatives under the control of the *GAL1* promoter from a low-copy plasmid were grown to mid-log phase (OD_{600} = 0.8 to 1.5) in SGal medium. In Fig. 5F, *tom40-97* cells expressing Cit1-HA or its mutant derivatives were grown in SRaf medium at 30°C until the OD_{600} reached approximately 6 to 9. The culture was then diluted 50-fold into SGal medium and further grown at 30°C until the OD_{660} reached 0.2 to 0.3, which was measured using a plate reader (Infinite 200 PRO, Tecan); this usually took ~1 day. In all cases, cells were treated with 0.05% azide and washed with distilled water before their pellets were stored at −80°C. To extract metabolites, cells were suspended in 100 μl of 70% methanol. Subsequently, the cells were heated at 100°C for 5 min and then agitated on a vortex mixer (TAITEC Max Mixer EVR-032) at room temperature for 5 min. The suspension was cleared by centrifugation at 20,000g for 2 min, and the supernatant (80 μl) was transferred to a new tube. Methanol was removed by evaporation at 55°C for 1 hour in a microcentrifugal vacuum concentrator (TOMY, MV-100). The dried pellet was dissolved in 500 μl of Milli-Q water, and the solution was passed through centrifugal filter units (Ultra-0.5 ml Amicon, catalog no. UFC501096) by centrifugation at 12,000 rpm for 10 min at room temperature to remove proteins. The cleared solution was subjected to the citrate assay (Sigma-Aldrich, catalog no. MAK057-1KT) according to the manufacturer's instructions.

Aggregation assay
In Fig. 4D, cells were grown in SRaf medium at 30°C overnight until OD_{600} reached 3 to 5. Cells were 10-fold diluted into the same medium and further grown at 30°C for 9 hours. Expression of NΔCit1-HA and its mutant variants was induced by adding 2% galactose to the medium. After 30 min, 10 OD_{600} equivalents of cells were collected and stored at −80°C. Cells were lysed in 300 μl of buffer [30 mM tris-HCl (pH 7.5), 20 mM KCl, 150 mM NaCl, and 5 mM EDTA] supplemented with 1× PIC using glass beads in a round-bottom plastic tube by eight rounds of vigorous vortexing for 30 s with 30-s intervals on ice. The same buffer (450 μl) was added, and the suspension was transferred to a new tube. The glass beads were washed again with 450 μl of buffer and pooled in the same tube. The resultant crude lysate was added to 1% Triton X-100 and stored on ice for 15 min. The lysate was cleared by centrifugation at 20,000g for 10 min at 4°C, and the supernatant was transferred to a new microfuge tube. Where indicated, the lysate was heated at 100°C ("boil"). A portion of the lysate (generally ~50 μl) was saved, trichloroacetic acid-precipitated, dissolved in

KNTCASB, and used as an input control. The remaining lysate (~800 μl) was subjected to ultracentrifugation at 100,000g for 1 hour at 4°C in a P50A3 rotor (himac, CP80NX). The supernatant was saved, trichloroacetic acid-precipitated, and dissolved in KNTCASB supplemented with an equal amount of 1 M tris (designated S100). The pellet fraction was dissolved in KNTCASB supplemented with 100 mM tris (designated P100). The volume of P100 and S100 samples was adjusted, and proteins that were derived from an equal number of cells were subjected to SDS-PAGE analysis after samples were heated at 55°C for 15 min and centrifuged for 1 min at room temperature.

In Fig. 5G, *tom40-97* cells harboring plasmids encoding Cit1-HA-DS/AA or Cit1-HA-DS/AA-H/G under the control of the *GAL1* promoter were grown in 15 ml of SRaf medium at 30°C. When the OD_{600} reached 0.8 to 1.0 (it generally took 18 to 19 hours), galactose was added at a final concentration of 2% to induce expression of Cit1-HA-DS/AA and Cit1-HA-DS/AA-H/G, the temperature was shifted to 33°C, and cells were further cultures for 2 hours. Subsequently, 10 OD_{600} equivalents of cells were collected by centrifugation at 3300 rpm for 2 min at room temperature using a KUBOTA s-722 rotor. Cells were directly lysed in 300 μl of buffer [30 mM tris-HCl (pH 7.5), 20 mM KCl, 150 mM NaCl, 5 mM EDTA, and 1% Triton X-100] supplemented with 1× PIC using glass beads in a round-bottom plastic tube by eight rounds of vigorous vortexing for 30 s with 30-s intervals on ice. The same buffer (450 μl) was then added, and the suspension was transferred to a new tube. The glass beads were washed once again with 450 μl of buffer and pooled in the same tube. Next, 900 μl of the lysate was transferred to a protein low-binding tube (WATSON, catalog no. PK-15C-500). The lysate was cleared by centrifugation at 300g for 3 min at 4°C, and the supernatant was further subjected to ultracentrifugation at 100,000g for 1 hour at 4°C in a P50A3 rotor (himac, CP80NX). The supernatant was harvested, trichloroacetic acid-precipitated, and dissolved in KNTCASB supplemented with an equal amount of 1 M tris (designated S100). The pellet fraction was rinsed with 900 μl of the same lysis buffer followed by centrifugation at 20,000g for 10 min before being dissolved in KNTCASB supplemented with 100 mM tris (designated P100). The volume of P100 and S100 samples was adjusted, and samples were processed as above.

Metabolome analysis
Sample preparation
Cells (BY4741) harboring a low-copy plasmid encoding NΔCit1-DS/AA or NΔCit1-DS/AA-H/G under the control of the *GAL1* promoter (comparison I) were grown in SD medium at 30°C overnight. The cells were then diluted 10,000- or 20,000-fold into SGal medium (three biological replicates for each strain) and grown at 30°C for ~40 hours until the OD_{600} reached approximately 0.7 to 0.8. Next, 10 OD_{600} equivalents of cells were collected. For metabolome analysis in *tom40-97* cells harboring a low-copy plasmid encoding Cit1-DS/AA or Cit1-DS/AA-H/G under the control of the *GAL1* promoter (comparison II), cells were grown in SRaf medium at 30°C for 3 days. The cells were then diluted 50-fold into SGal medium (three biological replicates for each strain) and grown at 30°C for ~24 hours until the OD_{600} reached approximately 1 to 2. Next, 10 OD_{600} equivalents of cells were collected. For metabolomic tracing analysis using ^{13}C-labeled galactose, cells were grown as described above, with the exception that they were cultured in SGal

medium containing ^{13}C-labeled galactose (Cambridge Isotope Laboratories Inc., catalog no. CLM-1570-0.1) for approximately 40 hours until the OD_{600} reached approximately 0.6 to 0.9 (BY4741 cells) or for ~24 hours until the OD_{600} reached approximately 0.7 to 0.9 (tom40-97 cells). Next, 0.7 OD_{600} equivalents of cells were collected. In all cases, cells were collected by vacuum filtration using vacuum filter holders (SHIBATA, catalog no. 061630 to 2501) and Omnipore membrane filters (Merck, catalog no. JHWP02500). Immediately after cells were washed with 5 ml of 50 mM ammonium acetate, the membrane filter with cells attached was transferred into 1.6 ml of −80°C methanol supplemented with 20 μM MES and 20 μM L-methionine sulfone and stored at −80°C until metabolite extraction. Subsequently, 640 μl of Milli-Q water and 1.6 ml of chloroform were added, and metabolites were extracted by vortexing for 1 min and sonicating for 1 min. The solution was cleared by centrifugation at 3300 rpm at 4°C for 10 min. The supernatant was then transferred to a new microcentrifuge tube, centrifuged at 15,000 rpm for 5 min at 4°C, and then subjected to centrifugal filtration through a 5-kDa cutoff filter (Merck, catalog no.UFC3LCCNB-HMT) to remove proteins.

IC-FTMS for anionic metabolite analysis

For metabolomic analysis focusing on glycolysis, the TCA cycle, the pentose phosphate pathway, and nucleotide metabolism, an Orbitrap mass spectrometer (Q-Exactive Focus, Thermo Fisher Scientific) was connected to a high-performance IC system (ICS-5000+, Thermo Fisher Scientific) to measure anionic metabolites. This system enabled efficient separation of ionic metabolites and highly selective and sensitive detection of metabolites using the principle of Fourier transform MS (FTMS) (76). The IC instrument was equipped with a modified anion electrolytic suppressor (Dionex AERS 500, Thermo Fisher Scientific) to convert the potassium hydroxide gradient to pure water before entering the mass spectrometer. Separation was performed post-column on a Dionex IonPac AS11-HC (4-μm particle size) column (Thermo Fisher Scientific) with an IC flow rate of 0.25 ml/min and methanol make-up flow of 0.18 ml/min. Potassium hydroxide gradient conditions for IC separations were 1 to 100 mM (0 to 40 min), 100 mM (40 to 50 min), and 1 mM (50 to 60 min); column temperature was 30°C. The Q Exactive Focus mass spectrometer was operated in electrospray ionization (ESI) negative mode for all detections. A full mass scan (mass/charge ratio 70 to 900) was used with a resolution of 70,000. The automatic gain control target was set to 3×106 ions with a maximum ion implantation time of 100 ms. Ion source parameters were optimized at a spray voltage of 3 kV, transfer temperature of 320°C, S-lens level of 50, heater temperature of 300°C, sheath gas of 36, and aux gas of 10. Relative amounts of metabolites were normalized using internal standard compounds.

LC-MS/MS analysis of cationic metabolite analysis

Cationic metabolite (amino acid) levels were quantified LC-tandem MS (LC-MS/MS). Briefly, a triple quadrupole mass spectrometer (LCMS-8040, Shimadzu, Kyoto, Japan) equipped with an ESI ion source was used in positive and negative ESI multiple reaction monitoring (MRM) mode. Samples were separated on a Discovery HS F5-3 column [2.1 mm inner diameter × 150 mm length, 3-μm particle, Sigma-Aldrich, St Louis, MO, USA) with mobile phase A (0.1% formate) and mobile phase B (0. 1% acetonitrile). Separation was performed using a step gradient of mobile phase A (0.1% formate) and mobile phase B (0. 1% acetonitrile) in ratios of 100:0 (0 to 5 min), 75:25 (5 to 11 min), 65:35 (11 to 15 min), 5:95

(15 to 20 min), and 100:0 (20 to 25 min), with a flow rate of 0.25 ml/min and a column temperature of 40°C. MRM conditions for each amino acid have been reported previously (77). The obtained metabolome dataset was subjected to pathway enrichment analysis using Metaboanalyst (www.metaboanalyst.ca/) software (78).

RNA sequencing

Cells (BY4741) expressing NΔCit1-DS/AA (termed 8A) or NΔCit1-DS/AA-H/G (termed 8I) under the control of the GAL1 promoter from a low-copy plasmid were grown in SGal medium (three biological replicates for each cell type). When the OD_{600} reached approximately 0.7 to 0.9 (which usually took approximately 24 to 32 hours), cells were collected by centrifugation at 3300 rpm for 2 min, washed with 1 ml of TBS buffer [20 mM tris-HCl (pH 7.5) and 150 mM NaCl], frozen in liquid nitrogen, and then stored at −80°C. RNA was extracted using the RNeasy Kit (QIAGEN KK, catalog no. 74104). RNA library preparations, sequencing reactions, and most statistical analyses were performed by Hokkaido System Science Co. Ltd. Briefly, RNA sequencing libraries were prepared using the NEBNext Ultra II Directional RNA Library Prep Kit for Illumina (NEB, Ipswich), following the manufacturer's instructions. The sequencing library was validated on the Agilent TapeStation (Agilent Technologies) and was quantified using a Qubit 2.0 Fluorimeter (Invitrogen) and quantitative polymerase chain reaction (KAPA Biosystems). The sequencing libraries were clustered on a single lane of a flow cell. After clustering, the flow cell was loaded on the Illumina NovaSeq 6000 instrument, according to the manufacturer's instructions. The samples were sequenced using a 2 × 150–base pair paired-end configuration. Sequence reads were trimmed to remove possible adaptor sequences and nucleotides with poor quality using Cutadapt v.1.8. The trimmed reads were quantified in mapping-based mode using Salmon v.1.2.1 based on the S. cerevisiae S288c reference transcripts available via ENSEMBL. After extraction of gene hit counts, the gene hit count table was used for downstream differential expression analysis. A comparison of gene expression between 8A and 8I cells was performed using Tag Count Comparison. The exact test (79) was used to generate q values and $\log_2$ fold changes. Genes with a q value < 0.05 were considered differentially expressed.

Puromycin incorporation assay

Some of the following methods are similar to those previously published (75). Cells (pdr5Δ) harboring a plasmid encoding NΔCit1-HA-DS/AA or NΔCit1-HA-DS/AA-H/G under the control of the GAL1 promoter were grown in 5 ml of SRaf medium at 30°C for 24 hours. The next day, the culture was diluted 10,000-fold in 10 ml of fresh medium and grown at 30°C overnight. Subsequently, galactose was added to the medium at a final concentration of 2%. After 8 hours, the cell density was adjusted to $OD_{600} = 0.5$ by adding SGal medium. Next, 900 μl of culture was added to 100 μl of puromycin dihydrochloride (2 mg/ml; FUJIFILM Wako, catalog no. 160 to 23151) (final concentration of 200 μg/ml) for 20 min at 30°C to label the nascent polypeptides. Where indicated, cells were treated with cycloheximide (100 μg/ml) for 5 min before the addition of puromycin. Cells were collected by centrifugation at 15,000 rpm for 1 min, and the cell pellet was stored at −80°C until use. To prepare whole-cell lysates, cells were incubated with 180 μl of 0.2 M NaOH at room temperature for 10 min, collected by centrifugation at 15,000 rpm for 1 min, suspended in 60 μl of 2× SDS-PAGE

sample buffer [120 mM tris-HCl (pH 7.5), 4% SDS, 20% glycerol, 0.05% BPB, and 6% 2-mercaptoethanol], and vortexed vigorously for 20 min at room temperature to extract proteins. Next, the samples were heated at 55°C for 20 min and cleared by centrifugation, and the supernatant was applied to an SDS-PAGE gel. Puromyclated proteins were detected by WB using an anti-puromycin antibody (COSMO BIO, catalog no. PEN-MA001).

Polysome analysis

Some of the following methods are similar to those previously published (75). Cells harboring a low-copy plasmid encoding NΔCit1-HA-DS/AA or NΔCit1-HA-DS/AA-H/G under the control of the *GAL1* promoter were grown in SRaf medium overnight and then diluted 5000-fold into SRaf medium. The next morning, when the OD_{600} reached approximately 0.1 to 0.4, 2% galactose was added to induce the expression of NΔCit1-HA-DS/AA or NΔCit1-HA-DS/AA-H/G. When the OD_{600} reached approximately 1.0 to 1.5, the cells were transferred to a conical tube with cycloheximide (final concentration of 100 μg/ml) on ice. All subsequent steps were performed at 4°C. The cells were centrifuged at 5000 rpm for 10 min in a KUBOTA A-5006 rotor and washed with 50 ml of water supplemented with cycloheximide (100 μg/ml). Subsequently, the cells were pelleted by centrifugation at 3300 rpm for 2 min at 4°C in a KUBOTA s-722 rotor. The cell pellet was transferred to a microcentrifuge tube and stored at −80°C until use. To generate a lysate, cells were resuspended in 500 μl of lysis buffer [50 mM tris-HCl (pH 7.5), 12 mM Mg(OAc)$_2$, and 100 mM KCl] supplemented with 1 mM DTT (FUJIFILM WAKO, catalog no. 048-29224), heparin sodium salt (50 μg/ml; Nacalai Tesque, catalog no. 17513-41), 1× PIC, cycloheximide (100 μg/ml), and 0.5% Triton X-100. The cell suspension was transferred to a 50-ml conical tube and lysed in the presence of one volume of zirconia beads (0.5 mm; YZB05, Yasui Kikai) by vortexing eight times for 30 s with 30-s intervals. Lysates were transferred to microcentrifuge tubes and cleared by centrifugation at 15,000 rpm for 10 min at 4°C. A portion of the supernatant was saved for quantification of proteins. The remaining supernatant was loaded onto a 10 to 50% linear sucrose gradient, which was prepared in lysis buffer supplemented with 0.1% Triton X-100. The gradient was prepared using a Gradient Master instrument (BioComp, Model 108), according to the manufacturer's instructions. Ultracentrifugation was performed in a SW41 rotor (Beckman Instruments) for 1.5 hours at 37,000 rpm. The gradients were collected from the top using a Piston Gradient Fractionator (BioComp). The UV absorbance at 254 nm (A_{254}) was measured continuously using a Bio-Mini UV monitor (AC-5100 L) to generate traces, which were analyzed using the WebPlotDigitizer tool and the Excel program. The saved supernatant was separated by SDS-PAGE and stained with CBB to measure the relative amounts of proteins. The y axis of the polysome profile was standardized to the relative amount of proteins that was ultracentrifuged.

Statistical analysis

ImageJ (NIH) was used for quantification of Western blot images. Statistical analyses were performed in GraphPad Prism 9 or Excel using two-tailed unpaired t tests or one-way analysis of variance (ANOVA) with Dunnett's or Bonferroni's multiple comparison test. Error bars represent the SE. Significance is indicated as follows: ns, not significant. *$P < 0.05$, **$P < 0.01$, ***$P < 0.001$, and ****$P < 0.0001$.

Supplementary Materials

This PDF file includes:
Figs. S1 to S7
Tables S1 and S2
Legend for table S3
References

Other Supplementary Material for this manuscript includes the following:
Table S3

View/request a protocol for this paper from *Bio-protocol*.

REFERENCES AND NOTES

1. N. Pfanner, B. Warscheid, N. Wiedemann, Mitochondrial proteins: From biogenesis to functional networks. *Nat. Rev. Mol. Cell Biol.* **20**, 267–284 (2019).

2. L. Drwesh, D. Rapaport, Biogenesis pathways of α-helical mitochondrial outer membrane proteins. *Biol. Chem.* **401**, 677–686 (2020).

3. Y. S. Bykov, D. Rapaport, J. M. Herrmann, M. Schuldiner, Cytosolic events in the biogenesis of mitochondrial proteins. *Trends Biochem. Sci.* **45**, 650–667 (2020).

4. Y. Araiso, K. Imai, T. Endo, Role of the TOM complex in protein import into mitochondria: Structural views. *Annu. Rev. Biochem.* **91**, 679–703 (2022).

5. F. Boos, L. Krämer, C. Groh, F. Jung, P. Haberkant, F. Stein, F. Wollweber, A. Gackstatter, E. Zöller, M. van der Laan, M. M. Savitski, V. Benes, J. M. Herrmann, Mitochondrial protein-induced stress triggers a global adaptive transcriptional programme. *Nat. Cell Biol.* **21**, 442–451 (2019).

6. C. U. Martensson, C. Priesnitz, J. Song, L. Ellenrieder, K. N. Doan, F. Boos, A. Floerchinger, N. Zufall, S. Oeljeklaus, B. Warscheid, T. Becker, Mitochondrial protein translocation-associated degradation. *Nature* **569**, 679–683 (2019).

7. S. Yablonska, V. Ganesan, L. M. Ferrando, J. Kim, A. Pyzel, O. V. Baranova, N. K. Khattar, T. M. Larkin, S. V. Baranov, N. Chen, C. E. Strohlein, D. A. Stevens, X. Wang, Y. F. Chang, M. E. Schurdak, D. L. Carlisle, J. S. Minden, R. M. Friedlander, Mutant huntingtin disrupts mitochondrial proteostasis by interacting with TIM23. *Proc. Natl. Acad. Sci. U.S.A.* **116**, 16593–16602 (2019).

8. H. Yano, S. V. Baranov, O. V. Baranova, J. Kim, Y. Pan, S. Yablonska, D. L. Carlisle, R. J. Ferrante, A. H. Kim, R. M. Friedlander, Inhibition of mitochondrial protein import by mutant huntingtin. *Nat. Neurosci.* **17**, 822–831 (2014).

9. F. J. B. Bäuerlein, I. Saha, A. Mishra, M. Kalemanov, A. Martínez-Sánchez, R. Klein, I. Dudanova, M. S. Hipp, F. U. Hartl, W. Baumeister, R. Fernández-Busnadiego, In situ architecture and cellular interactions of PolyQ inclusions. *Cell* **171**, 179–187.e10 (2017).

10. E. M. Szegő, A. Dominguez-Meijide, E. Gerhardt, A. König, D. J. Koss, W. Li, R. Pinho, C. Fahlbusch, M. Johnson, P. Santos, A. Villar-Piqué, T. Thom, S. Rizzoli, M. Schmitz, J. Li, I. Zerr, J. Attems, O. Jahn, T. F. Outeiro, Cytosolic trapping of a mitochondrial heat shock protein is an early pathological event in synucleinopathies. *Cell Rep.* **28**, 65–77.e6 (2019).

11. R. Di Maio, P. J. Barrett, E. K. Hoffman, C. W. Barrett, A. Zharikov, A. Borah, X. Hu, J. M. Coy, C. T. Chu, E. A. Burton, T. G. Hastings, J. T. Greenamyre, α-Synuclein binds to TOM20 and inhibits mitochondrial protein import in Parkinson's disease. *Sci. Transl. Med.* **8**, 342ra78 (2016).

12. V. Sorrentino, M. Romani, L. Mouchiroud, J. S. Beck, H. Zhang, D. D'Amico, N. Moullan, F. Potenza, A. W. Schmid, S. Rietsch, S. E. Counts, J. Auwerx, Enhancing mitochondrial proteostasis reduces amyloid-β proteotoxicity. *Nature* **552**, 187–193 (2017).

13. G. Cenini, C. Rub, M. Bruderek, W. Voos, Amyloid β-peptides interfere with mitochondrial preprotein import competence by a coaggregation process. *Mol. Biol. Cell* **27**, 3257–3272 (2016).

14. D. Mossmann, F.-N. Vögtle, A. A. Taskin, P. F. Teixeira, J. Ring, J. M. Burkhart, N. Burger, C. M. Pinho, J. Tadic, D. Loreth, C. Graff, F. Metzger, A. Sickmann, O. Kretz, N. Wiedemann, R. P. Zahedi, F. Madeo, E. Glaser, C. Meisinger, Amyloid-β peptide induces mitochondrial dysfunction by inhibition of preprotein maturation. *Cell Metab.* **20**, 662–669 (2014).

15. U. Nowicka, P. Chroscicki, K. Stroobants, M. Sladowska, M. Turek, B. Uszczynska-Ratajczak, R. Kundra, T. Goral, M. Perni, C. M. Dobson, M. Vendruscolo, A. Chacinska, Cytosolic aggregation of mitochondrial proteins disrupts cellular homeostasis by stimulating the aggregation of other proteins. *eLife* **10**, e65484 (2021).

16. S. Ravanelli, F. den Brave, T. Hoppe, Mitochondrial quality control governed by ubiquitin. *Front. Cell Dev. Biol.* **8**, 270 (2020).

17. C. Andréasson, M. Ott, S. Büttner, Mitochondria orchestrate proteostatic and metabolic stress responses. *EMBO Rep.* **20**, e47865 (2019).

18. X. Wang, X. J. Chen, A cytosolic network suppressing mitochondria-mediated proteostatic stress and cell death. *Nature* **524**, 481–484 (2015).

19. L. Wrobel, U. Topf, P. Bragoszewski, S. Wiese, M. E. Sztolsztener, S. Oeljeklaus, A. Varabyova, M. Lirski, P. Chroscicki, S. Mroczek, E. Januszewicz, A. Dziembowski, M. Koblowska, B. Warscheid, A. Chacinska, Mistargeted mitochondrial proteins activate a proteostatic response in the cytosol. *Nature* **524**, 485–488 (2015).

20. F. Boos, J. Labbadia, J. M. Herrmann, How the mitoprotein-induced stress response safeguards the cytosol: A unified view. *Trends Cell Biol.* **30**, 241–254 (2020).

21. J. Song, J. M. Herrmann, T. Becker, Quality control of the mitochondrial proteome. *Nat. Rev. Mol. Cell Biol.* **22**, 54–70 (2021).

22. M. B. Metzger, J. L. Scales, M. F. Dunklebarger, J. Loncarek, A. M. Weissman, A protein quality control pathway at the mitochondrial outer membrane. *eLife* **9**, e51065 (2020).

23. H. Weidberg, A. Amon, MitoCPR-A surveillance pathway that protects mitochondria in response to protein import stress. *Science* **360**, eaan4146 (2018).

24. T. Su, T. Izawa, M. Thoms, Y. Yamashita, J. Cheng, O. Berninghausen, F. U. Hartl, T. Inada, W. Neupert, R. Beckmann, Structure and function of Vms1 and Arb1 in RQC and mitochondrial proteome homeostasis. *Nature* **570**, 538–542 (2019).

25. O. Zurita Rendón, E. K. Fredrickson, C. J. Howard, J. Van Vranken, S. Fogarty, N. D. Tolley, R. Kalia, B. A. Osuna, P. S. Shen, C. P. Hill, A. Frost, J. Rutter, Vms1p is a release factor for the ribosome-associated quality control complex. *Nat. Commun.* **9**, 2197 (2018).

26. E. Itakura, E. Zavodszky, S. Shao, M. L. Wohlever, R. J. Keenan, R. S. Hegde, Ubiquilins chaperone and triage mitochondrial membrane proteins for degradation. *Mol. Cell* **63**, 21–33 (2016).

27. K. G. Hansen, N. Aviram, J. Laborenz, C. Bibi, A. Meyer, A. Spang, M. Schuldiner, J. M. Herrmann, An ER surface retrieval pathway safeguards the import of mitochondrial membrane proteins in yeast. *Science* **361**, 1118–1122 (2018).

28. V. P. Shakya, W. A. Barbeau, T. Xiao, C. S. Knutson, M. H. Schuler, A. L. Hughes, A nuclear-based quality control pathway for non-imported mitochondrial proteins. *eLife* **10**, e61230 (2021).

29. J. A. Schafer, S. Bozkurt, J. B. Michaelis, K. Klann, C. Munch, Global mitochondrial protein import proteomics reveal distinct regulation by translation and translocation machinery. *Mol. Cell* **82**, 435–446.e7 (2022).

30. L. P. Coyne, X. J. Chen, mPOS is a novel mitochondrial trigger of cell death - implications for neurodegeneration. *FEBS Lett.* **592**, 759–775 (2018).

31. S. Backes, Y. S. Bykov, T. Flohr, M. Räschle, J. Zhou, S. Lenhard, L. Krämer, T. Mühlhaus, C. Bibi, C. Jann, J. D. Smith, L. M. Steinmetz, D. Rapaport, Z. Storchová, M. Schuldiner, F. Boos, J. M. Herrmann, The chaperone-binding activity of the mitochondrial surface receptor Tom70 protects the cytosol against mitoprotein-induced stress. *Cell Rep.* **35**, 108936 (2021).

32. S. Haferkamp, K. Drexler, M. Federlin, H. J. Schlitt, M. Berneburg, J. Adamski, A. Gaumann, E. K. Geissler, V. Ganapathy, E. K. Parkinson, M. E. Mycielska, Extracellular citrate fuels cancer cell metabolism and growth. *Front. Cell Dev. Biol.* **8**, 602476 (2020).

33. M. Kunze, A. Hartig, Permeability of the peroxisomal membrane: Lessons from the glyoxylate cycle. *Front. Physiol.* **4**, 204 (2013).

34. K. Nakatsukasa, T. Nishimura, S. D. Byrne, M. Okamoto, A. Takahashi-Nakaguchi, H. Chibana, F. Okumura, T. Kamura, The ubiquitin ligase SCF(Ucc1) acts as a metabolic switch for the glyoxylate cycle. *Mol. Cell* **59**, 22–34 (2015).

35. J. R. Skaar, J. K. Pagan, M. Pagano, Mechanisms and function of substrate recruitment by F-box proteins. *Nat. Rev. Mol. Cell Biol.* **14**, 369–381 (2013).

36. S. Orlicky, X. Tang, A. Willems, M. Tyers, F. Sicheri, Structural basis for phosphodependent substrate selection and orientation by the SCFCdc4 ubiquitin ligase. *Cell* **112**, 243–256 (2003).

37. L. Holm, Dali server: Structural unification of protein families. *Nucleic Acids Res.* **50**, W210–W215 (2022).

38. B. Hao, S. Oehlmann, M. E. Sowa, J. W. Harper, N. P. Pavletich, Structure of a Fbw7-Skp1-cyclin E complex: Multisite-phosphorylated substrate recognition by SCF ubiquitin ligases. *Mol. Cell* **26**, 131–143 (2007).

39. G. Wu, G. Xu, B. A. Schulman, P. D. Jeffrey, J. W. Harper, N. P. Pavletich, Structure of a β-TrCP1-Skp1-β-catenin complex: Destruction motif binding and lysine specificity of the SCF$^{\beta-TrCP1}$ ubiquitin ligase. *Mol. Cell* **11**, 1445–1456 (2003).

40. B. Hao, N. Zheng, B. A. Schulman, G. Wu, J. J. Miller, M. Pagano, N. P. Pavletich, Structural basis of the Cks1-dependent recognition of p27(Kip1) by the SCF(Skp2) ubiquitin ligase. *Mol. Cell* **20**, 9–19 (2005).

41. Y. J. Lee, J. W. Jang, K. J. Kim, P. J. Maeng, TCA cycle-independent acetate metabolism via the glyoxylate cycle in *Saccharomyces cerevisiae*. *Yeast* **28**, 153–166 (2011).

42. C. T. Evans, L. C. Kurz, S. J. Remington, P. A. Srere, Active site mutants of pig citrate synthase: Effects of mutations on the enzyme catalytic and structural properties. *Biochemistry* **35**, 10661–10672 (1996).

43. L. C. Kurz, T. Nakra, R. Stein, W. Plungkhen, M. Riley, F. Hsu, G. R. Drysdale, Effects of changes in three catalytic residues on the relative stabilities of some of the intermediates and transition states in the citrate synthase reaction. *Biochemistry* **37**, 9724–9737 (1998).

44. C. Ratledge, Regulation of lipid accumulation in oleaginous micro-organisms. *Biochem. Soc. Trans.* **30**, 1047–1050 (2002).

45. X. Guo, N. M. Niemi, P. D. Hutchins, S. G. F. Condon, A. Jochem, A. Ulbrich, A. J. Higbee, J. D. Russell, A. Senes, J. J. Coon, D. J. Pagliarini, Ptc7p dephosphorylates select mitochondrial proteins to enhance metabolic function. *Cell Rep.* **18**, 307–313 (2017).

46. K. Gabriel, B. Egan, T. Lithgow, Tom40, the import channel of the mitochondrial outer membrane, plays an active role in sorting imported proteins. *EMBO J.* **22**, 2380–2386 (2003).

47. M. M. Desai, Statistical questions in experimental evolution. *J. Stat. Mech. Theory Exp.* **2013**, P01003 (2013).

48. M. van der Laan, A. Chacinska, M. Lind, I. Perschil, A. Sickmann, H. E. Meyer, B. Guiard, C. Meisinger, N. Pfanner, P. Rehling, Pam17 is required for architecture and translocation activity of the mitochondrial protein import motor. *Mol. Cell. Biol.* **25**, 7449–7458 (2005).

49. Z. Cai, Y. Deng, J. Ye, Y. Zhuo, Z. Liu, Y. Liang, H. Zhang, X. Zhu, Y. Luo, Y. Feng, R. Liu, G. Chen, Y. Wu, Z. Han, Y. Liang, F. Jiang, W. Zhong, Aberrant expression of citrate synthase is linked to disease progression and clinical outcome in prostate cancer. *Cancer Manag. Res.* **12**, 6149–6163 (2020).

50. B. Schlichtholz, J. Turyn, E. Goyke, M. Biernacki, K. Jaskiewicz, Z. Sledzinski, J. Swierczynski, Enhanced citrate synthase activity in human pancreatic cancer. *Pancreas* **30**, 99–104 (2005).

51. L. Chen, T. Liu, J. Zhou, Y. Wang, X. Wang, W. di, S. Zhang, Citrate synthase expression affects tumor phenotype and drug resistance in human ovarian carcinoma. *PLOS ONE* **9**, e115708 (2014).

52. H. C. Causton, B. Ren, S. S. Koh, C. T. Harbison, E. Kanin, E. G. Jennings, T. I. Lee, H. L. True, E. S. Lander, R. A. Young, Remodeling of yeast genome expression in response to environmental changes. *Mol. Biol. Cell* **12**, 323–337 (2001).

53. Z. Kuang, S. Pinglay, H. Ji, J. D. Boeke, Msn2/4 regulate expression of glycolytic enzymes and control transition from quiescence to growth. *eLife* **6**, e29938 (2017).

54. E. K. Schmidt, G. Clavarino, M. Ceppi, P. Pierre, SUnSET, a nonradioactive method to monitor protein synthesis. *Nat. Methods* **6**, 275–277 (2009).

55. J. R. Broach, Nutritional control of growth and development in yeast. *Genetics* **192**, 73–105 (2012).

56. A. Huber, S. L. French, H. Tekotte, S. Yerlikaya, M. Stahl, M. P. Perepelkina, M. Tyers, J. Rougemont, A. L. Beyer, R. Loewith, Sch9 regulates ribosome biogenesis via Stb3, Dot6 and Tod6 and the histone deacetylase complex RPD3L. *EMBO J.* **30**, 3052–3064 (2011).

57. S. I. Lippman, J. R. Broach, Protein kinase A and TORC1 activate genes for ribosomal biogenesis by inactivating repressors encoded by Dot6 and its homolog Tod6. *Proc. Natl. Acad. Sci. U.S.A.* **106**, 19928–19933 (2009).

58. I. Martinez-Reyes, N. S. Chandel, Mitochondrial TCA cycle metabolites control physiology and disease. *Nat. Commun.* **11**, 102 (2020).

59. P. K. Arnold, B. T. Jackson, K. I. Paras, J. S. Brunner, M. L. Hart, O. J. Newsom, S. P. Alibeckoff, J. Endress, E. Drill, L. B. Sullivan, L. W. S. Finley, A non-canonical tricarboxylic acid cycle underlies cellular identity. *Nature* **603**, 477–481 (2022).

60. K. Pakos-Zebrucka, I. Koryga, K. Mnich, M. Ljujic, A. Samali, A. M. Gorman, The integrated stress response. *EMBO Rep.* **17**, 1374–1395 (2016).

61. V. Iacobazzi, V. Infantino, Citrate – new functions for an old metabolite. *Biol. Chem.* **395**, 387–399 (2014).

62. J. Eniafe, S. Jiang, The functional roles of TCA cycle metabolites in cancer. *Oncogene* **40**, 3351–3363 (2021).

63. R. Yang, Y. Li, Y. Wang, J. Zhang, Q. Fan, J. Tan, W. Li, X. Zou, B. Liang, NHR-80 senses the mitochondrial UPR to rewire citrate metabolism for lipid accumulation in *Caenorhabditis elegans*. *Cell Rep.* **38**, 110206 (2022).

64. K. Nakatsukasa, T. Kawarasaki, A. Moriyama, Heterologous expression and functional analysis of the F-box protein Ucc1 from other yeast species in *Saccharomyces cerevisiae*. *J. Biosci. Bioeng.* **128**, 704–709 (2019).

65. M. Peng, D. Yang, Y. Hou, S. Liu, M. Zhao, Y. Qin, R. Chen, Y. Teng, M. Liu, Intracellular citrate accumulation by oxidized ATM-mediated metabolism reprogramming via PFKP and CS enhances hypoxic breast cancer cell invasion and metastasis. *Cell Death Dis.* **10**, 228 (2019).

66. E. Lionaki, I. Gkikas, I. Daskalaki, M.-K. Ioannidi, M. I. Klapa, N. Tavernarakis, Mitochondrial protein import determines lifespan through metabolic reprogramming and de novo serine biosynthesis. *Nat. Commun.* **13**, 651 (2022).

67. Z. Otwinowski, W. Minor, [20] Processing of X-ray diffraction data collected in oscillation mode. *Methods Enzymol.* **276**, 307–326 (1997).

68. A. J. McCoy, Solving structures of protein complexes by molecular replacement with *Phaser. Acta Crystallogr. D Biol. Crystallogr.* **63**, 32–41 (2007).

69. M. Biasini, S. Bienert, A. Waterhouse, K. Arnold, G. Studer, T. Schmidt, F. Kiefer, T. G. Cassarino, M. Bertoni, L. Bordoli, T. Schwede, SWISS-MODEL: Modelling protein tertiary and quaternary structure using evolutionary information. *Nucleic Acids Res.* **42**, W252–W258 (2014).

70. P. Emsley, B. Lohkamp, W. G. Scott, K. Cowtan, Features and development of *Coot. Acta Crystallogr. D Biol. Crystallogr.* **66**, 486–501 (2010).

71. P. V. Afonine, R. W. Grosse-Kunstleve, N. Echols, J. J. Headd, N. W. Moriarty, M. Mustyakimov, T. C. Terwilliger, A. Urzhumtsev, P. H. Zwart, P. D. Adams, Towards automated crystallographic structure refinement with phenix.refine. *Acta Crystallogr. D Biol. Crystallogr.* **68**, 352–367 (2012).

72. K. Cowtan, The Buccaneer software for automated model building. 1. Tracing protein chains. *Acta Crystallogr. D Biol. Crystallogr.* **62**, 1002–1011 (2006).

73. R. A. Laskowski, M. B. Swindells, LigPlot+: Multiple ligand–protein interaction diagrams for drug discovery. *J. Chem. Inf. Model.* **51**, 2778–2786 (2011).

74. S. Hayward, H. J. C. Berendsen, Systematic analysis of domain motions in proteins from conformational change: New results on citrate synthase and T4 lysozyme. *Proteins* **30**, 144–154 (1998).

75. K. Kusama, Y. Suzuki, E. Kurita, T. Kawarasaki, K. Obara, F. Okumura, T. Kamura, K. Nakatsukasa, Dot6/Tod6 degradation fine-tunes the repression of ribosome biogenesis under nutrient-limited conditions. *iScience* **25**, 103986 (2022).

76. S. Hu, J. Wang, E. H. Ji, T. Christison, L. Lopez, Y. Huang, Targeted metabolomic analysis of head and neck cancer cells using high performance ion chromatography coupled with a Q exactive HF mass spectrometer. *Anal. Chem.* **87**, 6371–6379 (2015).

77. M. Oka, K. Hashimoto, Y. Yamaguchi, S.-I. Saitoh, Y. Sugiura, Y. Motoi, K. Honda, Y. Kikko, S. Ohata, M. Suematsu, M. Miura, K. Miyake, T. Katada, K. Kontani, Arl8b is required for lysosomal degradation of maternal proteins in the visceral yolk sac endoderm of mouse embryos. *J. Cell Sci.* **130**, 3568–3577 (2017).

78. Z. Pang, G. Zhou, J. Ewald, L. Chang, O. Hacariz, N. Basu, J. Xia, Using MetaboAnalyst 5.0 for LC–HRMS spectra processing, multi-omics integration and covariate adjustment of global metabolomics data. *Nature Protocols* **17**, 1735–1761 (2022).

79. J. Sun, T. Nishiyama, K. Shimizu, K. Kadota, TCC: An R package for comparing tag count data with robust normalization strategies. *BMC Bioinformatics* **14**, 219 (2013).

80. R. S. Sikorski, P. Hieter, A system of shuttle vectors and yeast host strains designed for efficient manipulation of DNA in Saccharomyces cerevisiae. *Genetics* **122**, 19–27 (1989).

81. D. Mumberg, R. Muller, M. Funk, Yeast vectors for the controlled expression of heterologous proteins in different genetic backgrounds. *Gene* **156**, 119–122 (1995).